Minimum 1D Velocity Model and Local Magnitude Scale for Myanmar

Hasbi Ash Shiddiqi[1], Pa Pa Tun[2], Lars Ottemöller[1]

[1]Department of Earth Science, University of Bergen, Allègaten 41, N-5007 Bergen, Norway.

[2]Department of Meteorology and Hydrology, Office No. 5, Ministry of Transport and Communications, Zeya Htani Road, Nay Pyi Taw, Myanmar.

Abstract

Earthquake monitoring in Myanmar has improved in recent years due to an increased number of seismic stations. This provides a good quality dataset to derive a minimum 1D velocity model and local magnitude (M_L) scale for the Myanmar region, which will improve the earthquake location and magnitude estimates in this region. We combined and reprocessed earthquake catalogs from the Department of Meteorology and Hydrology of Myanmar (DMH) and the International Seismological Centre (ISC). Additional waveform data from various sources were processed as well. A total of 419 earthquakes were selected based on azimuthal gap, minimum number of stations and RMS travel-time residual. A set of initial seismic velocity models were derived from various seismic velocity models. These models were randomly perturbed and used as initial models in a coupled hypocenter and 1D seismic velocity inversion procedure. We compared the average mean travel-time residuals from the initial and inverted models. The best final model showed an improvement of location standard errors compared to the old model. Furthermore, the local magnitude scale inversion for the Myanmar region was performed using 194 earthquakes that have a minimum of two amplitude observations. The following M_L scale was obtained:

$$M_L = \log A\ (nm) + 1.485\ * \log R\ (km) + 0.00118 * R(km) - 2.77\ + S$$

This scale is valid for hypocentral distance up to 1000 km and magnitudes up to M_L=6.2.

Introduction

Myanmar falls into an active tectonic region situated between the Himalaya mountain belt and Sumatra-Andaman subduction zone. The earthquakes in the country are monitored by the Myanmar National Seismic Network which is operated by Department of Meteorology and Hydrology (DMH). The current earthquake location procedure is conducted using a preliminary 1D seismic velocity model.

It is still common to use 1D velocity models for routine earthquake location (e.g., Midzi et al. 2010; Husen et al. 2011), although it appears inappropriate in relatively complex tectonic region like Myanmar. There are several local 1D velocity models available in the surrounding region, e.g., Northeast India (Mukhopadhyay et al. 1997) and Bay of Bengal (Rao *et al.*, 2015). Several regional 3D seismic velocity models for the surrounding regions have also been developed (e.g., Li et al. 2008; Pesicek et al. 2008; Pesicek et al. 2010), however, these models have very few stations in Myanmar and are larger scale tomography models that have low resolution at depth shallower than 50 km for Myanmar region. There is, therefore, a need to derive a regional 1D seismic velocity model for Myanmar in order to improve the earthquake location accuracy.

Currently, DMH adopted the local magnitude (M_L) scale from Southern California (Hutton and Boore, 1987). The appropriate M_L scale for Myanmar will be useful to give a better estimate of the earthquake size and provide a better input for seismic hazard analysis.

In this study, we aim to develop a minimum 1D seismic velocity model for the Myanmar region by inverting a set of travel-time data for earthquakes in Myanmar and the surrounding regions. We selected different initial models from global velocity models and other studies from the Myanmar and the surrounding areas, and then we applied random perturbation to these initial models. A simultaneous inversion of 1D velocity and hypocenters was conducted using a set of initial models. Furthermore, we also aim to develop an M_L scale for the Myanmar region. The amplitude data from the vertical component of 15 stations were inverted to obtained the M_L distance correction term for Myanmar.

Tectonic and Seismicity in Myanmar

The convergence between the Indian and Burma plates created the Indo-Burman range (IBR) in the western part of Myanmar. The subducted Indian plate beneath this region is shown by the intermediate-depth seismicity down to about 150 km depth (see Figure 1) and the slab is clearly imaged by several teleseismic and regional seismic travel-time tomography studies with high P-wave velocity anomaly (e.g., Li et al. 2008; Pesicek et al. 2008; Pesicek et al. 2010; Raoof et al. 2017). The large scale regional and teleseismic tomography studies from Li et al. (2008) and Pesicek et al. (2008) show that the subducting Indian slab penetrates down to the mantle transition zone and then deflects around this depth to the east beneath Myanmar. A smaller scale seismic tomography illuminates the slab discontinuity between 50 to 100 km depth beneath the northern IBR (Raoof *et al.*, 2017). Hurukawa et al. (2012) showed that the strike of the subducted Indian slab is changing from north-northeast direction in the North to south-southeast in the South and the slab dip becomes steeper around the depth of ~50 to ~80 km.

The Sagaing fault, a major dextral strike-slip fault situated in the central part of the country (Figure 1), is a result of the highly oblique motion of the Indian plate relative to the Burma plate where the movement on the Sagaing Fault is about 18 mm/year (Socquet *et al.*, 2006). The Sagaing fault represents the boundary between the Burma Plate and the Sunda Plate (e.g., Le Dain et al. 1984; Ni et al. 1989). Several other active strike-slip faults are present in the Shan region of eastern Myanmar as a result of the extrusion-rotation of the northern part of the Sunda block (Wang *et al.*, 2014). The principal tectonics in the Myanmar region, as well as earthquakes and stations used in this study, are shown in Figure 1.

Before the 20th century, there were several records of historical earthquakes in Myanmar, e.g., the 1762 Arakan earthquake (Cummins, 2007; Gupta and Gahalaut, 2009). A number of shallow earthquakes related to the strike-slip faults across the country have caused damage (see also Aung (2017) for complete list). Hurukawa and Maung (2011) analyzed six $M \geq 7.0$ earthquakes that occurred around the Sagaing fault for the period between 1930 and 1956.

In recent years, shallow earthquakes have caused significant damage, e.g., the 2011 Mw=6.8 Tarlay earthquake in eastern Myanmar and the 2012 Mw=6.8 Shwebo earthquake in central Myanmar (Tun *et al.*, 2014; Wang *et al.*, 2014) (See Figure 1 for the location of the earthquakes). Some intermediate depth earthquakes also caused damage, especially around the IBR. Previous studies suggested that these earthquakes are a result of fault reactivation within the subducted slab (e.g., Kundu and Gahalaut 2012). In July 1975, an M_w(GCMT)=7.0 intermediate-depth earthquake (GCMT centroid depth = 95.7 km) struck central Myanmar, and caused severe damage to the old town of Bagan. In August 2016, an intra-slab M_w(GCMT)=6.8 (depth = 90 km) earthquake which also occurred at intermediate depth, occurred about 45 km south of the 1975 event (Shiddiqi *et al.*, 2018) (See Figure 1). This earthquake has also caused a minor damage in the old Bagan (Zaw *et al.*, 2017).

Seismic Monitoring in Myanmar

The earthquake monitoring in Myanmar dates back to 1963. The installation of the first analog seismographs was conducted in 1976 in Yangon and 1977 in Mandalay (Thiam *et al.*, 2017). The historic overview of seismic monitoring in Myanmar and the installation of five broadband stations by the U.S. Geological Survey and DMH were explained by Thiam et al. (2017). DMH is currently (January 2019) running 19 broadband seismic stations and 10 strong-motion stations that are collocated with some of the broadband stations. DMH is also using real-time data from broadband stations from the neighboring countries. For the real-time monitoring, DMH uses both the SeisComP3 (http://www.seiscomp3.org/; Weber et al. 2007) and Antelope software, while SEISAN (Havskov and Ottemoller, 1999; Ottemöller *et al.*, 2018) is used for interactive processing. SEISAN is configured to read continuous data from the SeisComP3 archive and to transfer event data into the database for further interactive processing.

Until 2013, DMH was mostly relying on the processing of analog seismograms. However, with the operation of digital stations there was a need to integrate data from different sources and to operate a common processing platform. To achieve this, DMH received technical and scientific support from the University of Bergen, Norway, under a project coordinated by the Asian Disaster Preparedness Center (ADPC) with funding from the Norwegian Ministry of Foreign Affairs. Between 2013 and 2017, various training activities were conducted in Myanmar and Norway including courses, workshops and research visits. The focus of the activities was hands-on training to solve practical problems within basic seismology, earthquake data processing, seismic hazard analysis, and instrumentation. SEISAN was adopted at DMH as the interactive processing tool to combine the various data sets and to store the processed data in a single event database.

Data

The DMH started to build an earthquake catalogue from 2014. The quality and completeness of this catalogue has been improving with the installation of new stations. We combined the DMH catalog with the Bulletin from the International Seismological Centre (ISC) for the region from January 2012 to April 2018. Furthermore, we re-picked the P- and S-wave arrivals with consistency from waveform data that are available from DMH, Incorporated Research Institutions for Seismology (IRIS), and the Observatories and Research Facilities for European Seismology (ORFEUS) European Integrated Data Archive (EIDA). We used data from permanent stations from the Myanmar National Seismic Network (MM), GEOFON Network (GE), Thai Seismic Monitoring Network (TM), National Seismic Network of India (IN), Bhutan Seismic Network (K5), China National Seismic Network, (CB), New China Digital Seismograph Network (IC), and Regional Integrated Multi-Hazard Early Warning System (RM). We also used the temporary networks, GANSSER broadband seismic experiment in Bhutan (XA) (Swiss Seismological Service (SED) at ETH Zurich, 2013) (six stations) and PIRE: Life on a tectonically active delta in Bangladesh (Z6) (one station). In total, this amounts to 76 stations in Myanmar and neighboring countries.

The data processing was conducted using the SEISAN software (Havskov and Ottemoller, 1999). The picked arrival times were combined with the reported arrival times from the ISC catalog. We also picked the maximum amplitude (in nanometers) of the S- or Lg waves of the simulated Wood-Anderson seismograms to obtain the local magnitudes of the earthquakes. We measured the zero-to-peak amplitude on the vertical components as that is the routine practice at DMH. To determine earthquake location and local magnitude, we used the HYPOCENTER program (Lienert *et al.*, 1986; Lienert and Havskov, 1995). Initially, we used the ak135 velocity model for continental structure (Kennett *et al.*, 1995) to perform the earthquake travel-time calculations. We removed the P- and S-arrival time data that have travel-time residuals greater than 2.0 seconds and 3.0 seconds, respectively, and then located the earthquakes again with cleaned the P- and S-arrival times.

To ensure the quality of earthquake location, we selected the earthquakes based on several criteria: 1) the earthquake is recorded by a minimum of eight stations, 2) the RMS travel-time residuals are less than 2.0 seconds, 3) the maximum azimuthal gap is 170º. We selected 419 earthquakes that passed the criteria for further analysis. In total, the dataset consisted of 5163 P-wave arrivals and 3583 S-wave arrivals. The ray-paths of the events mostly cover the entire Myanmar except for the southwest region since it lacks both stations and earthquakes (Figure 2.a and 2.b).

1D velocity model

The minimum 1D seismic velocity was inverted for simultaneously with hypocenter locations and station corrections by using the VELEST program (Ellsworth, 1978; Kissling *et al.*, 1994). The seismic travel-time problem is a non-linear problem of seismic velocity model along the ray-path and the earthquake locations (Kissling *et al.*, 1994). The quality of the 1D velocity model solution depends on earthquake location quality. This problem is referred to as coupled hypocenter-velocity problem, where the 1D velocity model is solved simultaneously with hypocenter locations (Kissling *et al.*, 1994). The inversion is linearized to solve the problem in a least square sense. It is essential to assign an appropriate number of layers and their thicknesses since VELEST does not invert for these. Hence, the appropriate initial seismic velocity model and high quality P- and S-arrival time dataset are essential input.

Initial velocity models

In the absence of a specific velocity model for earthquake location in Myanmar, we built starting models based on various global models: Crust 1.0 (Laske *et al.*, 2012) and the ak135 velocity model (Kennett *et al.*, 1995). We constructed an initial 1D velocity model Crust1.0 (referred to as MC1.0) by averaging the Vp and Vs for each layer and layer thicknesses for the study region. Below the Moho, velocities are not defined in Crust1.0 and we extracted values from ak135. The ak135 velocity model is also used as an initial model.

Wang et al. (2018) developed a 3D S-wave velocity model using a temporary network concentrated in the Central Myanmar and other temporary and permanent networks in the surrounding regions. They applied a joint inversion of receiver functions, surface wave dispersion measurements and H/V amplitude ratio of Rayleigh waves combined with velocities from Crust1.0 (referred to as Myanmar-Hybrid1 (MH1)) (Wang *et al.*, 2018). We calculated the average velocity for each layer of MH1 to create an initial 1D S-wave velocity model and combine it with 1D P-wave velocity model from Crust1.0. In addition, a 1D model from Northeast India from Raoof (et al. 2017) which was inverted using the VELEST program is also adopted (will be referred to as NEI Model). The NEI model was derived from local and regional data mostly from Northeast India and the surrounding regions including the Himalaya region, IBR region and northern Thailand. This model comprises a larger area than our study and there were only few arrival-time data from stations inside Myanmar. Mantle velocities from ak135 were combined with MH1 and NEI models. For each model, we constructed a model with a sedimentary layer (low velocity layer as the first layer) and a model without a sedimentary layer. The list of all initial velocity models used in this study is shown in Table 1 and the initial models are plotted in Figure S1.

Inverting for a 1D velocity model in a complex tectonic region like Myanmar is not an easy task, since there is huge variability in crustal thicknesses where the recent study from Wang et al. (2018) shows that the average crustal thickness around central Myanmar is around 30 km, and increases up to 35 km toward eastern Myanmar and IBR. In the northern part of Myanmar toward Tibet and Northeast India, the crustal thickness increases up to more than 50 km (Singh *et al.*, 2017). We obtained average crustal thickness of 37.5 km from MH1 model and 35 km from Crust1.0 model. However, Singh et al. (2017) showed the crustal thickness estimation from a receiver functions study in India and the surrounding region differs about up to 10 km compared to Crust1.0 model.

Inversion for velocity model

Since the layer thicknesses are not inverted, first we tested the layer thicknesses by dividing the crust into 5 km layers and added two 5 km thick layers below the expected Moho to test the Moho depth as suggested by Kissling et al. (1995). The velocities for these layers are interpolated from the original models, and the velocities increase with depth. To improve earthquake location, in every first iteration the hypocenters were relocated, and in every second iteration the velocity model inversion is conducted simultaneously with hypocenter relocation. This process is repeated for 20 iterations. Finally, the layers with similar velocities are merged. Based on this analysis, we determined the average crustal thicknesses for Myanmar in MH1 and MH1_sed model at 42.5 km and for other models, the crustal thickness is 45 km. We tested sedimentary thickness of of 2, 5, and 10 km for the models with the sedimentary layers.

We conducted a random initial model test to find our best velocity model. This was done by creating 500 perturbations for each model by randomly modifying each Vp and Vs in every layer within the range of ± 10 %, and we keep the Vp/Vs ratio within the range of 1.6 to 1.9. Each initial model is then inverted using VELEST. We adopted damping parameters suggested by Kissling et al. (1994), i.e. origin time damping = 0.01, hypocenter damping = 0.01, depth damping = 0.01, velocity damping = 1.0, and station correction damping = 1.0. The maximum number of iteration was set to 20.

We only accepted the inverted models with the lowest 10% of travel-time RMS residuals for each set of initial models. The final velocity models are obtained by averaging the accepted models. The distribution of inversion results for each model will give an indication of the inversion robustness. The results for all models are shown in Figure 3. This test showed that the initial models with sedimentary layer produced a relatively high uncertainty especially in the crust.

Our next step was to refine the station corrections by using the final velocity models from the first step and set a higher damping value for the velocity model (Husen *et al.*, 2011). In this case, the velocity model will not change significantly while the inversion updates the station corrections and hypocenters. Following Husen et al. (2011), we set a damping of 10.0 for the velocity model. The NPW station, located in Nay Pyi Taw (Figure 8.a) was used as reference station for station corrections, because it is located roughly in the center of the study area, and is operated during most of the period.

To assess the quality of the inversion result, we located the events with HYPOCENTER using the new velocity models along with the station corrections. Then, we compared the RMS travel-time residuals for each velocity model. The relocated events using models with sedimentary layers produced higher mean travel-time residual than the initial locations (Table 2). Based on the average weighted RMS travel-time residuals, the new 1D velocity model from ak135 and NEI gave the lowest values (Figure 4, Table 3). In the Discussion, we look at the estimation of the standard errors of hypocenter locations using these models. Furthermore, VELEST only uses the first arriving P- and S-waves, while in earthquake monitoring at DMH, the analysts also use other crustal phases to locate shallow earthquakes, e.g., Pn, Pg, Sn, and Sg. In the Discussion, we also show that when using these crustal phases for shallow earthquake location, the result using the new velocity model improves the earthquake locations.

Local magnitude inversion

Currently, DMH is using the Southern California local magnitude scale (Hutton and Boore, 1987). This may be a reasonable starting point as both areas are tectonically active. The tectonic settings are still quite different and it is important to test whether the Southern California scale may be appropriate, or if it is necessary to replace with a new scale derived for Myanmar that would provide better estimation of earthquake magnitude.

The local magnitude scale (M_L) was first introduced by Richter (1935) to estimate the size of earthquakes by measuring the maximum amplitude from the horizontal component seismogram recorded by the Wood-Anderson (WA) seismograph. This method is still widely used for local earthquake monitoring because of its simplicity and widespread use. Since this magnitude scale was introduced using the WA seismograph, today's digital seismogram is transformed into the equivalent of the WA recording with a period of 0.8 s and a damping factor of 0.8 (Havskov and Ottemöller, 2010; Ottemöller and Sargeant, 2013).

Richter (1935) introduced the M_L as

$$M_L = \log A - \log A0 + S \qquad (1)$$

in which A is the amplitude from the WA seismograph in mm, -log A0 is the epicentral distance dependent correction term, and S is the station correction. Bakun and Joyner (1984) later developed the M_L scale for Central California and introduced the correction term as

$$-\log A0 = a \log\left(\frac{R}{100}\,km\right) + b(R - 100\,km) + 3.0 \qquad (2)$$

where a and b are the parameters that depend on geometrical spreading and attenuation, respectively. R is the hypocentral distance in kilometers. Hutton and Boore (1987) obtained the constants a = 1.11 and b = 0.00189 for Southern California.

Inserting equation (2) into (1), and converting the WA peak amplitude in mm into peak amplitude in nanometers with unit gain instead of 2080 for original WA instrument, M_L scale for Southern California is,

$$M_L = \log A \ (\text{nm}) + 1.110 \log R \ (\text{km}) + 0.00189R - 2.09 \qquad (3)$$

where the constants a and b from Hutton & Boore (1987) are used (IASPEI, 2013). Since different tectonic and geological conditions yield different attenuation, it is important to use the appropriate correction terms to obtain the appropriate M_L. In order to obtain the M_L scale for Myanmar region, we use the following equation

$$M_L = \log A \ (\text{nm}) + a \log(R) \ (\text{km}) + bR + C + S \qquad (4)$$

We invert for M_L, a, b, the base level C, and S using the singular value decomposition method. This inversion follows the method described in Ottemöller and Sargeant (2013) and is implemented in the MAG2 program in the SEISAN package (Havskov and Ottemoller, 1999; Ottemöller *et al.*, 2018).

Inversion and Result

We used the earthquake catalog from January 2014 to April 2018 with the updated locations obtained in this work and selected only the stations that are used by DMH for real-time earthquake monitoring. The events that are used for this inversion have a minimum of two amplitude readings. We only used earthquakes that were shallower than 50 km. The total number of earthquakes is 194 which are recorded by a total of 15 stations. The number of S- and Lg-waves maximum amplitudes is 891. The ray-path coverage of the events used for the M_L inversion is shown in Figure 2.c.

The distribution of data with respect to distance and the old M_L is shown in Figure 6. We used the amplitudes with hypocentral distance less than 1000 km, while most of the hypocentral distances are within 100 to 400 km. The magnitude range is from M_L=1.0 to M_L=6.2. The tectonic settings of the East and Central and the West region of Myanmar are different. Earthquakes in the East and Central regions occur in the crust, while in western Myanmar or the IBR region, earthquakes occur from shallow crustal depth down to intermediate depth. However, our objective at this stage is to obtain a single magnitude scale for the whole region.

We obtained the following M_L scale for Myanmar:

$$M_L = \log A + 1.485 * \log R + 0.00118 * R - 2.77 + S \quad (5)$$

Furthermore, we also conducted another inversion where a and b values are fixed to the Southern California scale, and only invert for the station corrections. We compared the residuals of M_L obtained by using the Southern California scale without and with the stations corrections, the new M_L for Myanmar with station corrections (Figure 6). Both the M_L scale for Southern California and Myanmar with station corrections have much lower residuals compared to the Southern California scale without stations corrections, which suggests that local site variations significantly affect the maximum amplitudes.

Discussions

Minimum velocity model and earthquake location tests

To improve earthquake location in Myanmar, we inverted for a 1D velocity model using a catalog based on DMH and ISC data. We tested the inversion using different initial velocity models. The results from initial models with sedimentary layer gave the highest residuals. This is probably due to the difference of sedimentary thickness in the Myanmar region. The random initial models test showed that the velocity models with sedimentary layer produced quite large uncertainties especially for the velocities in the crust (Figure 4). Therefore, we decided not to use the velocity model with a sedimentary layer and sedimentary thickness in Myanmar can be accommodated by using station corrections.

After testing different initial models, the ak135, and NEI models produce the best results. Since these two models produced similar residuals, we estimated the standard errors of these models using bootstrap resampling analysis for 276 events recorded by at least 10 stations. We did the bootstrap analysis by adding random Gaussian noise with a standard error of 1.0 second to the arrival times in the earthquake catalog and then located the earthquakes using the initial and new models, and at every run, 10% of the data are excluded from the inversion. This process was repeated 200 times. Then, we calculated the horizontal and vertical standard errors of each event for these models (Figure 7). The lowest horizontal and depth standard errors were produced by the locations obtained using the final model from NEI. Therefore, we chose the final model from NEI as the best model and will be referred to as Myanmar Minimum 1D Velocity model (MM_1D) (Figure 5).

The low standard errors for the hypocenters located using the MM_1D model can be attributed to unevenly distributed earthquakes and stations throughout the study region. The majority of the earthquakes are located around the IBR, and many of the stations are also located around IBR and Northeast India region. This condition may explain the tendency of the MM_1D model to produce the smallest hypocentral standard errors compared to other models. On the other hand, the MH1 model was mostly derived using temporary stations mainly distributed in Central Myanmar, where there are only few earthquakes in our dataset. Figure 3 shows that the velocity models below the Moho tend to converge into smaller velocity range which indicates smaller velocity uncertainties. The earthquakes with depth below the Moho (45 km) make up 53% of the data set and are located mostly beneath the IBR. We can assume that the P- and S-waves travel through similar heterogeneities. As for the crustal part, the huge crustal thickness and velocity variations, and unevenly distributed crustal earthquakes can make velocities in the crustal layers difficult to resolve. Hence, our result produces higher uncertainty for the crustal models.

The station corrections for P-wave travel-times are shown in Figure 8.a and the station corrections for P-waves and S-waves are shown in Figure S2. The station corrections depict the difference between observed and calculated travel-times, where positive and negative values correspond to late and early observed arrival times, respectively (e.g., Wright, 2008; Midzi *et al.*, 2010). Most of the stations in the center of the study area have relatively small residuals except MDY, which has a station correction of -0.98 seconds. MDY is located on hard-rock (Thiam *et al.*, 2017), which make this station tend to have faster observed travel-time. There are other stations that have relatively large station corrections (>1 second), however we do not have any information about station site condition. Stations around the IBR have positive station corrections which can be attributed to the local site conditions or lateral velocity anomaly beneath this region. Since most of the earthquakes recorded by these stations are from the subducted slab, the upgoing seismic waves probably encounter low velocity anomaly beneath the IBR. A seismic tomography by Raoof et al. (2017) showed the existence of a low Vp anomaly beneath the IBR region down to ~ 40 km, which was interpreted as sediment metamorphosis at greater depth. There are also several stations in the east which have quite large travel time corrections (> 1.5 seconds). We suspect, that there are due to some misidentified phases included from the ISC catalog. Most of the earthquakes that were recorded by these stations are shallow earthquakes at regional distances, and in some cases the first arriving Pn phases are not easily picked, and sometimes Pg phases are identified as the first arriving phases.

We conducted a test to see whether the new model can produce relatively good hypocenter locations of events which have more relaxed constraints (e.g., fewer number of stations and larger azimuthal gap). We also tested if the location solutions improve when additional regional phases are used (e.g., Pg and Sg) in addition to the first arriving P- and S-waves, especially for the small shallow earthquakes where there is no station within a radius of 100 km.

For the first test, we compared the hypocenter solutions using the initial velocity model (ak135) and the final velocity model along with the station corrections. A total of 649 earthquakes were selected by using relaxed criteria, i.e., minimum number of stations: seven stations, maximum azimuthal gap: 200^{o}, and RMS travel-time residuals$\leq$ 3.5 seconds. The hypocenter locations using the initial velocity model (ak135) and the MM_1D model will be referred to as old hypocenters and new hypocenters, respectively. To estimate the standard errors of the old and final hypocenters, we also did the bootstrap resampling test. The 95th percentile (P_{95}) of final horizontal standard errors is slightly reduced compared to the old locations where the P_{95} for final hypocenter is 5.11 km while it is 6.21 km for the old locations. The vertical standard errors for final locations are significantly reduced, where the P_{95} for final hypocenters is 13.73 km and for the old hypocenters is 20.05 km. The cross-section plot of the old and final locations is shown in the supplementary material (Figure S3).

In the second test, we compared the mainshock and aftershocks of the Mw(USGS)=6.0 Phyu earthquake at 10 km depth that struck the southern region of Myanmar on 11 January 2018 . The mechanism of this event was oblique thrust. This earthquake occurred about 20 km from the Sagaing fault. DMH reported that the event was followed by more than 50 aftershocks at shallow depths. The closest stations are the NPW and YGN stations, both about 160 km from the epicenter (see Figure 8a). In order to reduce the depth uncertainty especially for the smaller events, we picked the crustal phases, e.g., Pg and Sg. We selected 28 earthquakes recorded by a minimum of five stations and with an azimuthal gap < 210^{o}. We then located the events using the HYPOCENTER program using two velocity models, i.e., the initial velocity model (ak135) and the MM_1D velocity model along with the station corrections (Figure 9).

Most of the initial locations have depth less than 10 km, where some of the depths are close to zero due to the layer boundary resulting in minimum RMS error. The initial epicenter distribution shows an east-west trend, however, there is no clear pattern in the cross-section view. On the other hand, the new locations show a pattern with the dip around 40^{o} to 50^{o}, which is quite consistent with the focal mechanism of the mainshock (Figure 9). The mainshock depth using the final model is 10.4 km. We also plotted horizontal location uncertainty by using error ellipses obtained from the inversion as well as the vertical uncertainty. Both of the horizontal and vertical uncertainties of the final locations are reduced significantly compared to the old location uncertainties (Figure 9).

M_L amplitude-distance curve for Myanmar and ML-mb(ISC) comparison

The M_L scale for Myanmar is obtained using the new seismic network data in Myanmar and the surrounding regions. Based on the dataset, this scale is valid for M_L up to 6.2 and distance up to 1000 km. We compared the M_L distance correction term ($a * \log R + b * R + c$) obtained in this study with the correction terms for other regions, i.e. Southern California (Hutton and Boore, 1987), Central California (Bakun and Joyner, 1984), Eastern U.S. (Kim, 1998), and Norway (Alsaker *et al.*, 1991) (Figure 10). The M_L distance correction term for Myanmar for the distance up to about 100 km is smaller than the Southern California scale. However, this is based only on about 60 observations. For distances greater than 100 km up to 400 km, where we have the most observations, the correction is slightly higher than the Southern California scale. As for the distances greater than 500 km the correction term become increasingly lower as the distance increases.

The residuals of M_L are significantly reduced if the new M_L scale is used together with station corrections (Figure 8.b). The sedimentary thickness is one of the factors that affects ground motion, even though we used the vertical components for amplitude reading, some variations are still expected. The amplitude used in the M_L scale introduced by Richter (1935) are measured on the horizontal components, however the common routine practice at DMH is to use the vertical components. Therefore, we decided to only measure the amplitudes on the vertical components. The Mandalay (MDY) and Myitkyina (MYI) stations have relatively large positive station corrections which suggests that the amplitudes on these stations are much lower than expected. As mentioned before, Thiam et al. (2017) reported that the MDY station is located on hard-rock and has low site amplification. As for the MYI station, we do not have any information about the site condition.

Even though the new M_L scale for Myanmar and the Southern California scale with station corrections produced similar residuals, the M_L values can be different. The a and b value are also different which reflects the different crustal conditions between Myanmar and Southern California. In most cases, the differences between these two magnitudes are mostly about ±0.1 magnitude units (m.u.), but the differences can reach up -0.2 m.u. (Figure S4). Therefore we suggest the usage of the new M_L scale instead of the Southern California scale for Myanmar region.

Since the new M_L scale for Myanmar was derived for shallow earthquakes, we tested the M_L calculation for deeper earthquakes, which are mostly intra-slab earthquakes (deeper than 50 km). Despite having larger residuals than shallow earthquakes, the residuals for M_L of deeper events are still within an acceptable range (Figure S6). Therefore, we suggest that for routine location procedure in Myanmar, the new M_L scale can be used for deeper earthquakes.

The new M_L scale for Myanmar is compared with the teleseismic body-wave magnitude m_b reported in the ISC bulletin. 73 events in our dataset are reported in the reviewed ISC catalog for the period between January 2014 to August 2016. A linear orthogonal regression between M_L and m_b (ISC) for 73 common events is m_b (ISC) = 1.08 M_L – 0.18 with scatter of 0.23 m.u. The regression indicates that the two magnitudes converge at magnitude 2.25, but m_b (ISC) is greater than M_L at large magnitudes (see Figure S6). The mean of M_L for 73 events is 4.25±0.63, whereas corresponding mean of m_b (ISC) is 4.43±0.68, and hence m_b is about 0.18 m.u. greater than M_L (Figure S5).

Conclusions

We have demonstrated that the new seismic velocity model and local magnitude scale along with the station corrections produced better locations and local magnitude estimates than what was obtained with current models. The MM_1D produces more accurate hypocenter solutions compared with other models tested in this study. When locating shallow earthquakes by using different crustal phases (Pn, Pg, Sg, and Sn), the use of the MM_1D model reduced the depth uncertainties of shallow earthquakes. The new M_L scale in Myanmar together with the station corrections produces lower residuals than the Southern California scale.

Further improvement is possible in the future, since Myanmar is a complex tectonic region where strong lateral variation exist, specific 1D velocity models and probably specific M_L scale can be developed for the different regions in Myanmar. As the Myanmar Seismic Network and the earthquakes database grow, there will be a good enough dataset to derive such models in the future.

Data and Resources

The local catalog data used in this study were provided by the Department of Meteorology and Hydrology of Myanmar. Additional data were downloaded from The International Seismological Centre (http://www.isc.ac.uk/, last accessed July 2018). Waveform data were obtained from Department of Meteorology and Hydrology of Myanmar, Incorporated Research Institutions for Seismology (IRIS), and the Observatories and Research Facilities for European Seismology (ORFEUS) European Integrated Data Archive (EIDA). The Obspy python package (Beyreuther *et al.*, 2010) was used to obtained some of the waveform data. Some of the figures were created using the Generic Mapping Tools (www.soest.hawaii.edu/gmt, last accessed

December 2017; Wessel et al. 2013). The topography data of EOTOPO.1 Global Relief model was used in Figure 1 and was obtained from https://www.ngdc.noaa.gov/mgg/global/ (last accessed September 2018). The ITRF2008 (Altamimi *et al.*, 2012) velocity vector in Figure 1 was obtained from UNAVCO Plate Motion Calculator (https://www.unavco.org/software/geodetic-utilities/plate-motion-calculator/plate-motion-calculator.html, last accessed May 2019). The topography data of Shuttle Radar Topography Mission (SRTM) 1 Arc-Second Global model was used in Figure 9. The SRTM model is available from the U.S. Geological Survey and was downloaded via https://earthexplorer.usgs.gov/ (last accessed, September 2018).

Acknowledgements

This research was conducted under "Seismic Monitoring, Myanmar II Project" which is funded by The Royal Norwegian Ministry of Foreign Affairs. The authors are grateful to Won-Young Kim for providing comments on the manuscript and to Felix Halpaap for the help on obtaining and managing waveform and catalog data. We thank Editor-in-Chief Zhigang Peng for his suggestions and his effort in handling this article and two anonymous reviewers for their constructive comments. We also thank our project partners, Asian Disaster Preparedness Center (ADPC) and Department of Meteorology and Hydrology (DMH), Ministry of Transport and Communication, Myanmar for their support during this project.

References

Alsaker, A., L. B. Kvamme, R. A. Hansen, A. Dahle, and H. Bungum (1991). The ML scale in Norway, *Bull. Seismol. Soc. Am.* **81**, no. 2, 379–398.

Altamimi, Z., L. Métivier, and X. Collilieux (2012). ITRF2008 plate motion model, *J.*

Geophys. Res. Solid Earth **117**, no. 7, 1–14, doi: 10.1029/2011JB008930.

Aung, H. H. (2017). *Myanmar Earthquakes History*, Myanmar Engineering Society, Yangon.

Bakun, W. H., and W. B. Joyner (1984). The ML scale in central California, *Bull. Seismol. Soc. Am.* **74**, no. 5, 1827–1843.

Beyreuther, M., R. Barsch, L. Krischer, T. Megies, Y. Behr, and J. Wassermann (2010). ObsPy: A Python Toolbox for Seismology, *Seismol. Res. Lett.* **81**, no. 3, 530–533.

Cummins, P. R. (2007). The potential for giant tsunamigenic earthquakes in the northern Bay of Bengal., *Nature* **449**, no. 9, 75–78, doi: 10.1038/nature06088.

Le Dain, Y. A., P. Tapponnier, and P. Molnar (1984). Active faulting and tectonics of Burma and surrounding regions, *J. Geophys. Res.* **89**, no. B1, 453–472, doi: 10.1029/JB089iB01p00453.

Ellsworth, W. L. (1978). Three-dimensional structure of the crust and mantle beneath the island of Hawaii., Ph.D. Thesis, Massachusetts Institute of Technology (http://hdl.handle.net/1721.1/52834, last accessed February 2019).

Gupta, H., and V. Gahalaut (2009). Is the northern Bay of Bengal tsunamigenic?, *Bull. Seismol. Soc. Am.* **99**, no. 6, 3496–3501, doi: 10.1785/0120080379.

Havskov, J., and L. Ottemoller (1999). SeisAn Earthquake Analysis Software, *Seismol. Res. Lett.* **70**, no. 5, 532–534.

Havskov, J., and L. Ottemöller (2010). *Routine Data Processing in Earthquake Seismology*, Springer, New York.

Hurukawa, N., and P. M. Maung (2011). Two seismic gaps on the Sagaing Fault, Myanmar, derived from relocation of historical earthquakes since 1918, *Geophys. Res. Lett.* **38**, no. 1, 1–5, doi: 10.1029/2010GL046099.

Hurukawa, N., P. P. Tun, and B. Shibazaki (2012). Detailed geometry of the subducting Indian Plate beneath the Burma Plate and subcrustal seismicity in the Burma Plate derived from joint hypocenter relocation, *Earth, Planets Sp.* **64**, no. 4, 333–343, doi: 10.5047/eps.2011.10.011.

Husen, S., E. Kissling, and J. F. Clinton (2011). Local and regional minimum 1D models for earthquake location and data quality assessment in complex tectonic regions: Application to Switzerland, *Swiss J. Geosci.* **104**, no. 3, 455–469, doi: 10.1007/s00015-011-0071-3.

Hutton, L. K., and D. M. Boore (1987). The Ml Scale in Southern California, *Bull. Seismol. Soc. Am.* **77**, no. 6, 2074–2094.

IASPEI (2013). Summary of Magnitude Working Group Recommendations on Standard Procedures for Determining Earthquake Magnitudes from Digital Data. http://iaspei.org/_Resources/Persistent/3de00aeb67e3ff2e6e78472357cd2899c633edea/Summary_WG_recommendations_20130327.pdf (la.

Kennett, B. L. N., E. R. Engdahl, and R. Buland (1995). Constraints on seismic velocities in the Earth from traveltimes, 108–124.

Kim, W.-Y. (1998). The ML scale in eastern North America, *Bull. Seismol. Soc. Am.* **88**, no. 4, 935–951.

Kissling, E. (1995). *Program Velest user's guide - Short Introduction*, Institute of Geophysics, ETH Zurich.

Kissling, E., W. L. L. Ellsworth, D. Eberhart-Phillips, and U. Kradolfer (1994). Initial reference models in local earthquake tomography, *J. Geophys. Res.* **99**, no. B10, 19635–19646.

Kundu, B., and V. K. Gahalaut (2012). Earthquake occurrence processes in the Indo-Burmese wedge and Sagaing fault region, *Tectonophysics* **524**–**525**, 135–146, doi: 10.1016/j.tecto.2011.12.031.

Laske, G., G. Masters, Z. Ma, and M. E. Pasyanos (2012). CRUST1.0: An Updated Global Model of Earth's Crust, in *Geophysical Research Abstracts EGU General Assembly,* 2012–3743.

Li, C., R. D. van der Hilst, A. S. Meltzer, and E. R. Engdahl (2008). Subduction of the Indian lithosphere beneath the Tibetan Plateau and Burma, *Earth Planet. Sci. Lett.* **274**, no. 1–2, 157–168, doi: 10.1016/j.epsl.2008.07.016.

Lienert, B. R., E. Berg, and L. N. Frazer (1986). Hypocenter: an Earthquake Location Method Using Centered, Scaled, and Adaptively Damped Least Squares, *Bull. Seismol. Soc. Am.* **76**, no. 3, 771–783.

Lienert, B. R., and J. Havskov (1995). A Computer Program for Locating Earthquakes Both Locally and Globally, *Seismol. Res. Lett.* **66**, no. 5, 26–36, doi: 10.1785/gssrl.66.5.26.

Midzi, V., I. Saunders, M. B. C. Brandt, and T. Molea (2010). 1-D Velocity Model for Use by the SANSN in Earthquake Location, *Seismol. Res. Lett.* **81**, no. 3, 460–466, doi: 10.1785/gssrl.81.3.460.

Mukhopadhyay, S., R. Chander, and K. N. Khattri (1997). Crustal properties in the epicentral tract of the Great 1897 Assam Earthquake, northeastern India, *Tectonophysics* **283**, no. 1, 311–330, doi: https://doi.org/10.1016/S0040-1951(97)00148-0.

Ni, J. F., M. Guzman-Speziale, M. Bevis, W. E. Holt, T. C. Wallace, and W. R. Seager (1989). Accretionary tectonics of Burma and the three-dimensional geometry of the Burma subduction zone, *Geology* **17**, no. 1, 68–71, doi: 10.1130/0091-7613(1989)017<0068:ATOBAT>2.3.CO;2.

Ottemöller, L., and S. Sargeant (2013). A local magnitude scale ML for the United Kingdom, *Bull. Seismol. Soc. Am.* **103**, no. 5, 2884–2893, doi: 10.1785/0120130085.

Ottemöller, L., P. Voss, and J. Havskov (2018). SEISAN: Earthquake Analysis Software, Department of Earth Science, University of Bergen, Bergen.

Pesicek, J. D., C. H. Thurber, S. Widiyantoro, E. R. Engdahl, and H. R. DeShon (2008). Complex slab subduction beneath northern Sumatra, *Geophys. Res. Lett.* **35**, no. 20, L20303, doi: 10.1029/2008GL035262.

Pesicek, J. D., C. H. Thurber, S. Widiyantoro, H. Zhang, H. R. DeShon, and E. R. Engdahl (2010). Sharpening the tomographic image of the subducting slab below Sumatra, the Andaman Islands and Burma, *Geophys. J. Int.* **182**, no. 1, 433–453, doi: 10.1111/j.1365-246X.2010.04630.x.

Rao, C. N., N. P. Rao, M. R. Kumar, S. Prasanna, and D. Srinagesh (2015). Structure and Tectonics of the Bay of Bengal through Waveform Modeling of the 21 May 2014 Earthquake of Magnitude 6.0, *Seismol. Res. Lett.* **86**, no. 2A, 378–384.

Raoof, J., S. Mukhopadhyay, I. Koulakov, and J. R. Kayal (2017). 3-D seismic tomography of the lithosphere and its geodynamic implications beneath the northeast India region, *Tectonics* **36**, no. 5, 962–980, doi: 10.1002/2016TC004375.

Richter, C. F. (1935). An instrumental earthquake magnitude scale, *Bull. Seismol. Soc. Am.*

25, no. 1, 1–32.

Shiddiqi, H. A., P. P. Tun, T. L. Kyaw, and L. Ottemöller (2018). Source Study of the 24 August 2016 Mw 6.8 Chauk, Myanmar, Earthquake, *Seismol. Res. Lett.* **89**, no. 5, 1773–1785, doi: 10.1785/0220170278.

Singh, A., M. Ravi Kumar, D. D. Mohanty, C. Singh, R. Biswas, and D. Srinagesh (2017). Crustal Structure Beneath India and Tibet: New Constraints From Inversion of Receiver Functions, *J. Geophys. Res. Solid Earth* **122**, no. 10, 7839–7859, doi: 10.1002/2017JB013946.

Socquet, A., C. Vigny, N. Chamot-Rooke, W. Simons, C. Rangin, and B. Ambrosius (2006). India and Sunda plates motion and deformation along their boundary in Myanmar determined by GPS, *J. Geophys. Res. Solid Earth* **111**, no. 5, 1–11, doi: 10.1029/2005JB003877.

Swiss Seismological Service (SED) at ETH Zurich (2013). GANSSER broadband seismic experiment in Bhutan, ETH Zurich. Other/Seismic Network. (https://doi.org/10.12686/sed/networks/xa, last accessed February 2019).

Thiam, H. N., Y. M. Min Htwe, T. L. Kyaw, P. P. Tun, Z. Min, S. H. Htwe, M. M. M. Aung, K. K. Lin, M. M. M. Aung, D. Cristofaro, *et al.* (2017). A Report on Upgraded Seismic Monitoring Stations in Myanmar: Station Performance and Site Response, *Seismol. Res. Lett.* **88**, no. 3, 1–9, doi: 10.1785/0220160168.

Tun, S. T., Y. Wang, S. N. Khaing, M. Thant, N. Htay, Y. Myo Min Htwe, T. Myint, and K. Sieh (2014). Surface ruptures of the Mw 6.8 march 2011 tarlay earthquake, Eastern Myanmar, *Bull. Seismol. Soc. Am.* **104**, no. 6, 2915–2932, doi: 10.1785/0120130321.

Wang, Y., K. Sieh, S. T. Tun, K.-Y. Lai, and T. Myint (2014). Active tectonic and earthquake Myanmar region, *J. Geophys. Res. Solid Earth* **119**, no. 4, 3767–3822, doi: 10.1002/2013JB010762.Received.

Wang, X., S. Wei, Y. Wang, P. Maung Maung, J. Hubbard, P. Banerjee, H. Bor-Shouh, K. Moe Oo, T. Bodin, A. Foster, *et al.* (2018). A 3D Shear‐Wave Velocity Model for Myanmar Region, *J. Geophys. Res. Solid Earth*, 1–23, doi: 10.1029/2018JB016622.

Weber, B., J. Becker, W. Hanka, A. Heinloo, M. Hoffmann, T. Kraft, D. Pahlke, J. Reinhardt, and H. Thoms (2007). SeisComP3 - automatic and interactive real time data processing, in *Geophysical Research Abstracts EGU General Assembly*, 09219.

Wessel, P., W. H. F. Smith, R. Scharroo, J. Luis, and F. Wobbe (2013). Generic mapping tools: improved version released, *EOS Trans AGU* **94**, doi: 10.1002/2013eo450001.

Wright, C. (2008). Station corrections for the Kaapvaal seismic network: Statistical properties and relation to lithospheric structure, *Phys. Earth Planet. Inter.* **167**, no. 1, 39–52, doi: https://doi.org/10.1016/j.pepi.2008.02.003.

Zaw, S. H., T. Ornthammarath, and N. Poovarodom (2017). Seismic reconnaissance and observed damage after the Mw 6.8, 24 August 2016 Chauk (Central Myanmar) earthquake, *J. Earthq. Eng.* **2469**, no. August, 13632469.2017.1323050-13632469.2017.1323050, doi: 10.1080/13632469.2017.1323050.

Figure Captions:

Figure 1. The distribution of earthquakes used in this study (circles colored according to the depths). Seismic stations (triangles) used in this study: 1. Seismic stations used in real-time seismic monitoring by Department of Meteorology and Hydrology of Myanmar (blue), 2. Other seismic stations that waveforms are available to this study (gray), 3. Seismic stations only with travel-time data only (black). Damaging earthquakes mentioned in the text are shown as black stars labelled with the year of occurrence. Active faults in Myanmar and the surrounding regions are depicted by black lines. The slip direction of Sagaing fault is shown by red arrows. Velocity vector is ITRF 2008 (Altamimi et al. 2012) velocity of Indian plate relative to Eurasian plate. The insert map is the area of study (black rectangle) in larger scale map.

Figure 2. a. The P-waves ray-path coverage of 419 earthquakes (circles) used in 1D seismic velocity inversion, b. The S-waves ray-path coverage. c. The ray-path coverage of 194 earthquakes used in M_L scale inversion (MAG2). d. Data distribution with respect of the Southern California M_L scale (Hutton and Boore 1987) and distance.

Figure 3. An example of the inversion step using the NEI model: a. The initial model with 5 km layer thicknesses in the crust and 10 km thickness in the mantle, b. The refined initial model which is obtained by inverting the initial model and combine the layers with similar velocities, c) the initial models for the random initial test, d. the result of random initial test where all inverted models are depicted by gray lines, and the accepted models are depicted by black lines.

Figure 4. The accepted results from the random initial test. The final velocity models are depicted with black lines, and all the accepted results from random test are shown as gray lines. a. The result for models without sedimentary layers, b. The result for models with sedimentary layers.

Figure 5. a. The plot of Vp and Vs versus depth of final model (MM_1D). b. The histogram that shows the depth distribution of the events used in the inversion.

Figure 6. M_L residuals with respect of distances (left) and M_L residuals vs number of observations (right): for Southern California scale (Hutton and Boore 1987) without station corrections (a) and with station corrections (b), and M_L derived in this study with station corrections (c).

Figure 7. a. Histogram of horizontal location standard error for the initial and the final from ak135 and NEI velocity models. The 95th percentile (P_{95}) of each models is also shown on the upper right of the figures. b. Histogram of vertical location standard error for the initial and the final velocity models.

Figure 8. a. P-wave travel-time corrections obtained from VELEST. The reference station (NPW) is depicted with a gray diamond. b. M_L station corrections. The stations discussed in the text are labelled.

Figure 9. a. The hypocenters distribution (with epicentral error ellipses) of the 11 January 2018 Phyu earthquake and its aftershocks located using the initial model (ak135). The focal mechanism is the solution from Global CMT. The east-west cross-section view is shown at the bottom. The vertical bars are proportional with the depth error of the events. Thick black line

is the topographic projection. b. the hypocenters distribution located using the final (MM_1D) velocity model.

Figure 10. Comparison of M_L correction term for unit of displacement in nanometers from this study and other regions. Below the curves, histogram of number of data used at different hypocentral distances is also shown.

Table Captions

Table 1. The list of initial 1D velocity models used in this study.

Table 2. The comparison of initial and final models mean residuals.

Table 3. Final Velocity model.

Tables

No	Velocity Model	Source	Comments
1	ak135	ak135	Without Sedimentary layer
2	ak135sed	ak135	With Sedimentary layer
3	MC1.0	Crust1.0 and ak135	Without Sedimentary layer
4	MC1.0sed	Crust1.0 and ak135	With Sedimentary layer
5	NEI	1D model from Raoof et al. (2017) and ak135	Without Sedimentary layer
6	NEIsed	1D model from Raoof et al. (2017) and ak135	With Sedimentary layer
7	MH1	Myanmar Hybrid model v1 (Wang et al., 2018), Crust1.0 and ak135	Without Sedimentary layer
8	MH1sed	Myanmar Hybrid model v1 (Wang et al., 2018), Crust1.0 and ak135	With Sedimentary layer

Table 1. The list of initial 1D velocity models used in this study.

No	Velocity Model	Initial mean residual (s)	Final mean residual (s)
1	ak135	1.286	1.085
2	ak135sed	1.272	1.519
3	MC1.0	1.269	1.244
4	MC1.0sed	1.246	1.386
5	NEI	1.255	1.084
6	NEIsed	1.289	1.647
7	MH1	1.307	1.200
8	MH1sed	1.3	1.278

Table 2. The comparison of initial and final models mean residuals.

Top layer depth (km)	Vp (km/s)	Vs (km/s)
above 0	5.58	3.31
15	6.10	3.32
25	6.62	3.83
45	8.07	4.65
65	8.19	4.66
80	8.19	4.70
120	8.53	4.72
165	8.70	4.83

Table 3. Final Velocity model.

Figure1

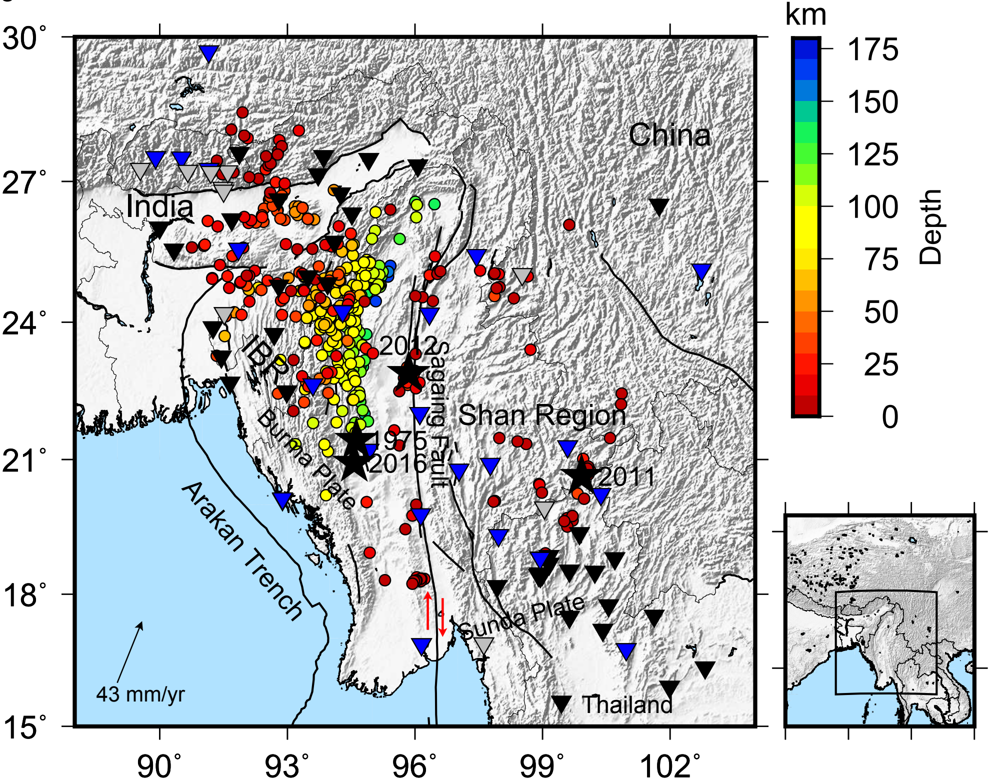

km
175
150
125
100
75
50
25
0
Depth
30°
27°
24°
21°
18°
15°
90°
93°
96°
99°
102°
China
India
IBR
2012
Sagaing Fault
Shan Region
1975
2016
2011
Burma Plate
Arakan Trench
Sunda Plate
Thailand
43 mm/yr

Figure2

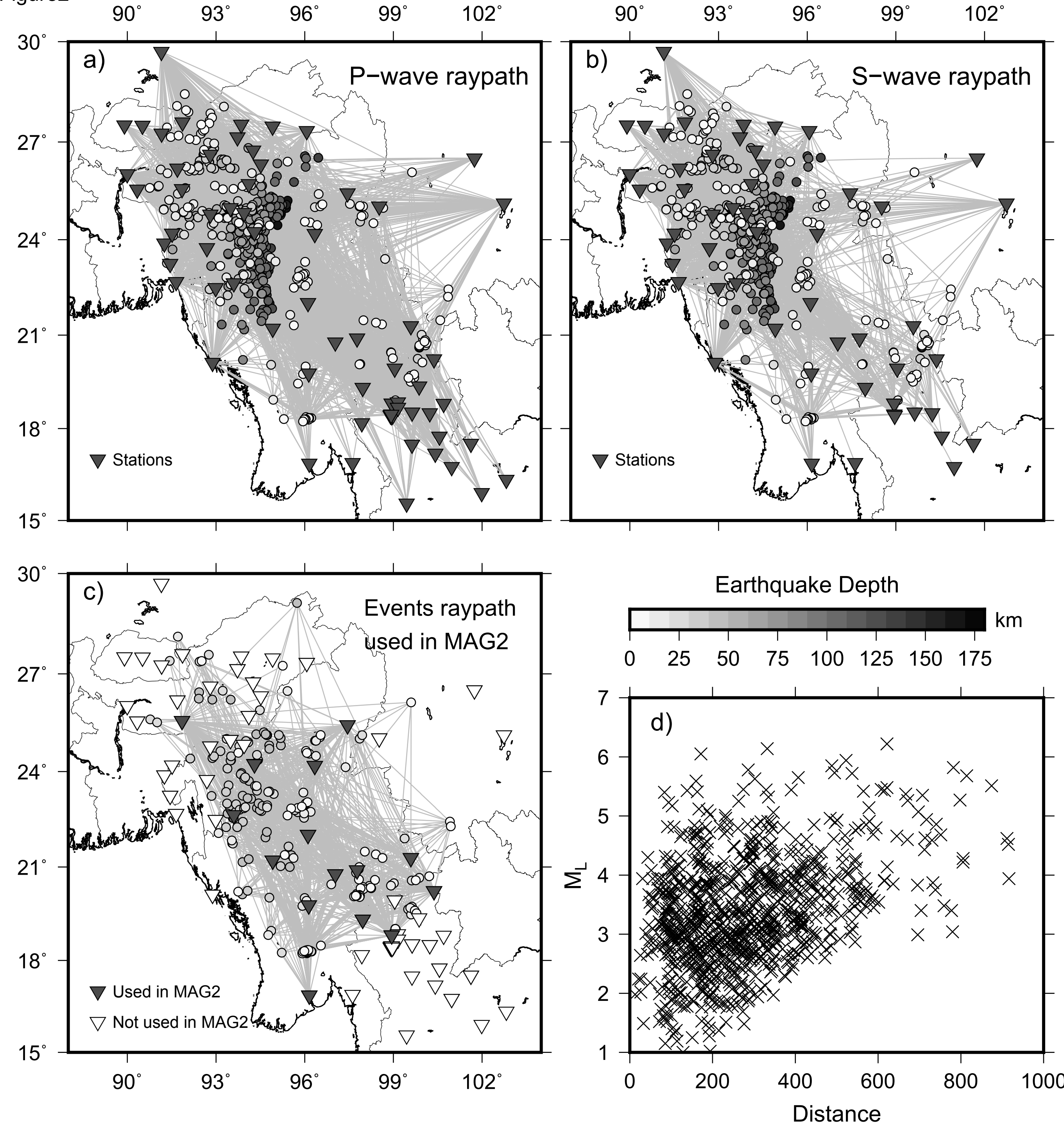

a)
P−wave raypath
Stations
b)
S−wave raypath
Stations
c)
Events raypath
used in MAG2
Used in MAG2
Not used in MAG2
Earthquake Depth
km
0 25 50 75 100 125 150 175
d)
M_L
Distance

Figure3

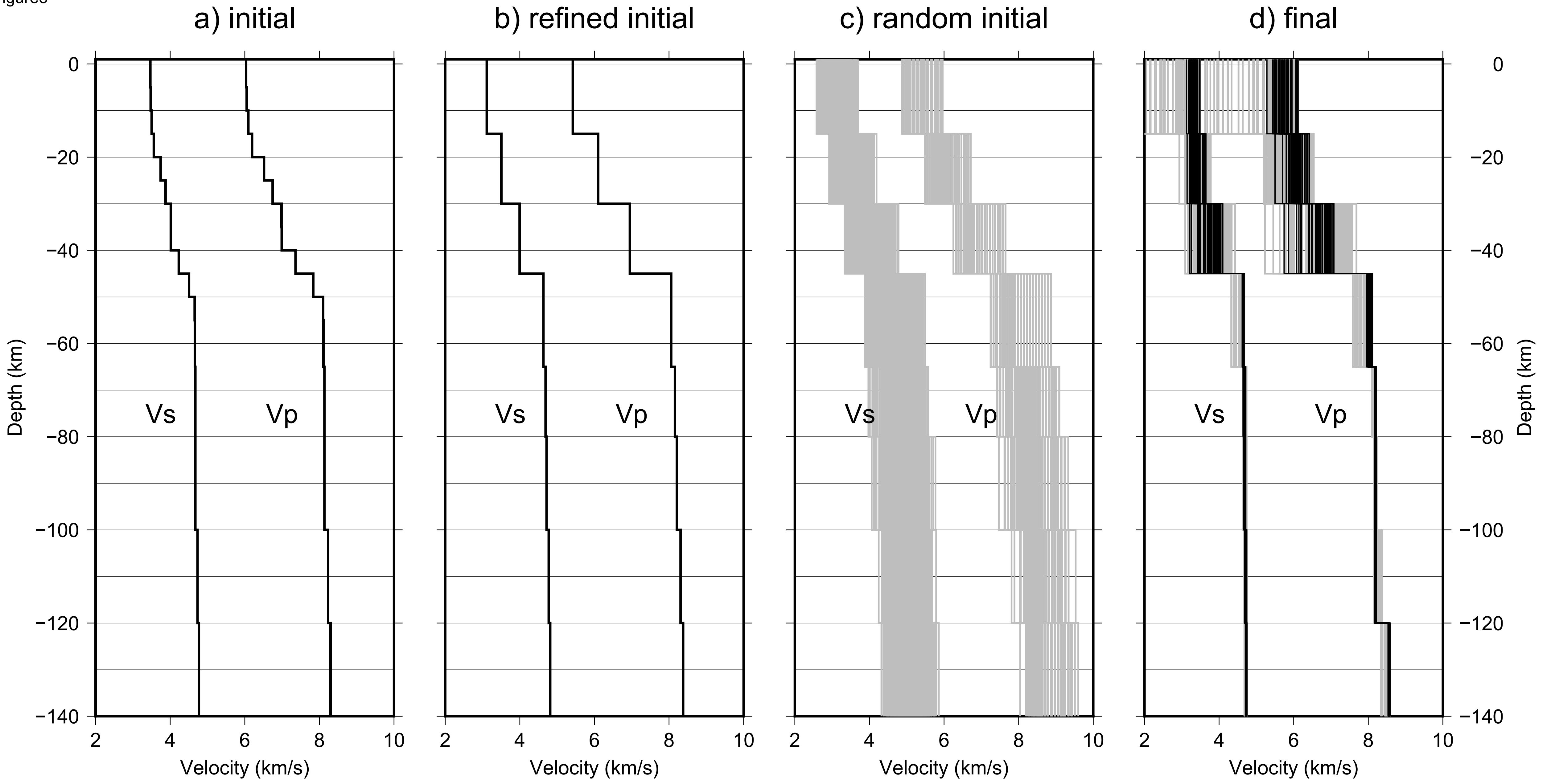

a) initial
b) refined initial
c) random initial
d) final
Depth (km)
0
−20
−40
−60
−80
−100
−120
−140
Vs
Vp
Velocity (km/s)
2
4
6
8
10

Figure4

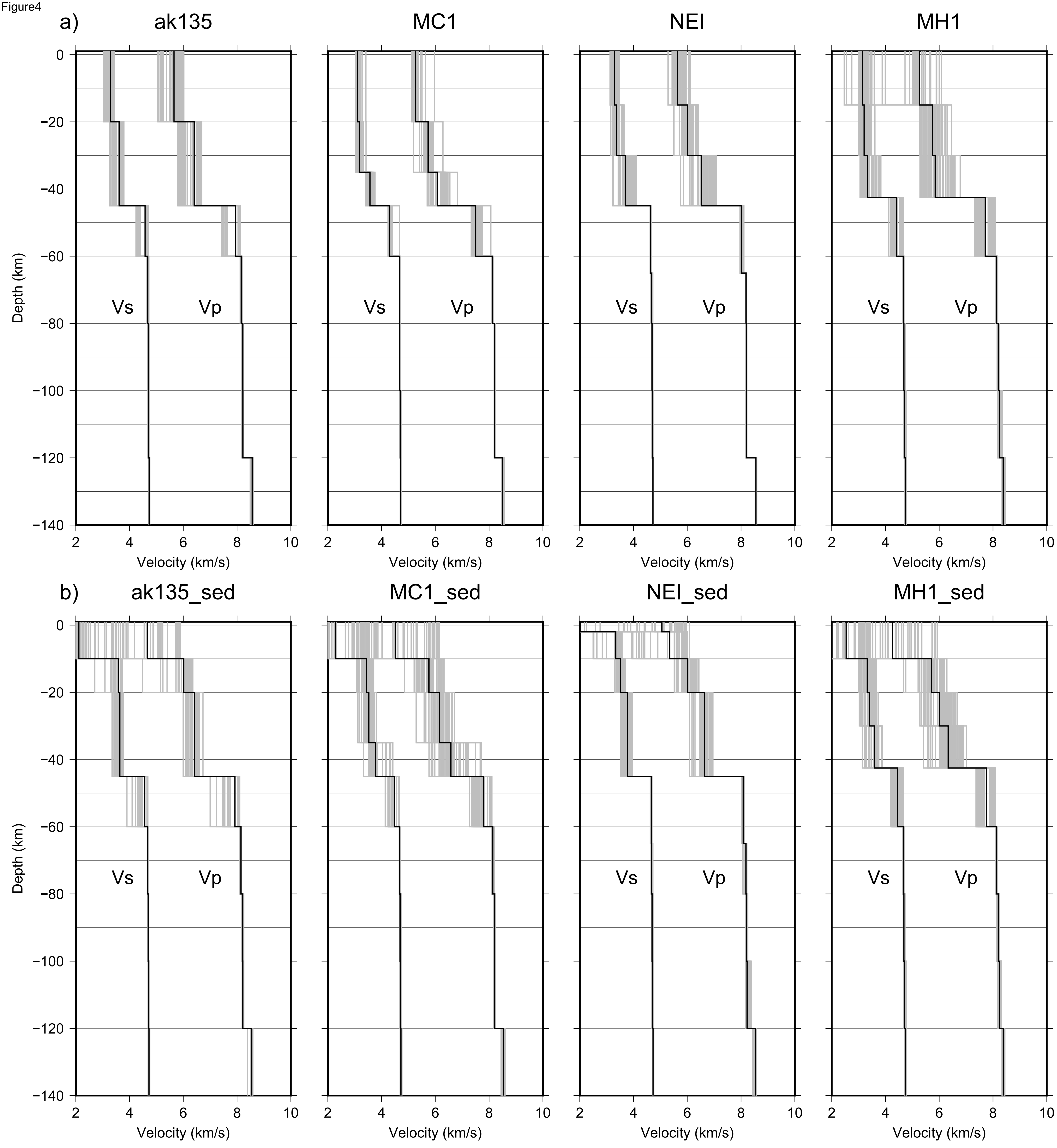

a)
ak135
MC1
NEI
MH1
b)
ak135_sed
MC1_sed
NEI_sed
MH1_sed
Vs
Vp
Depth (km)
Velocity (km/s)
0
-20
-40
-60
-80
-100
-120
-140
2
4
6
8
10

Figure5

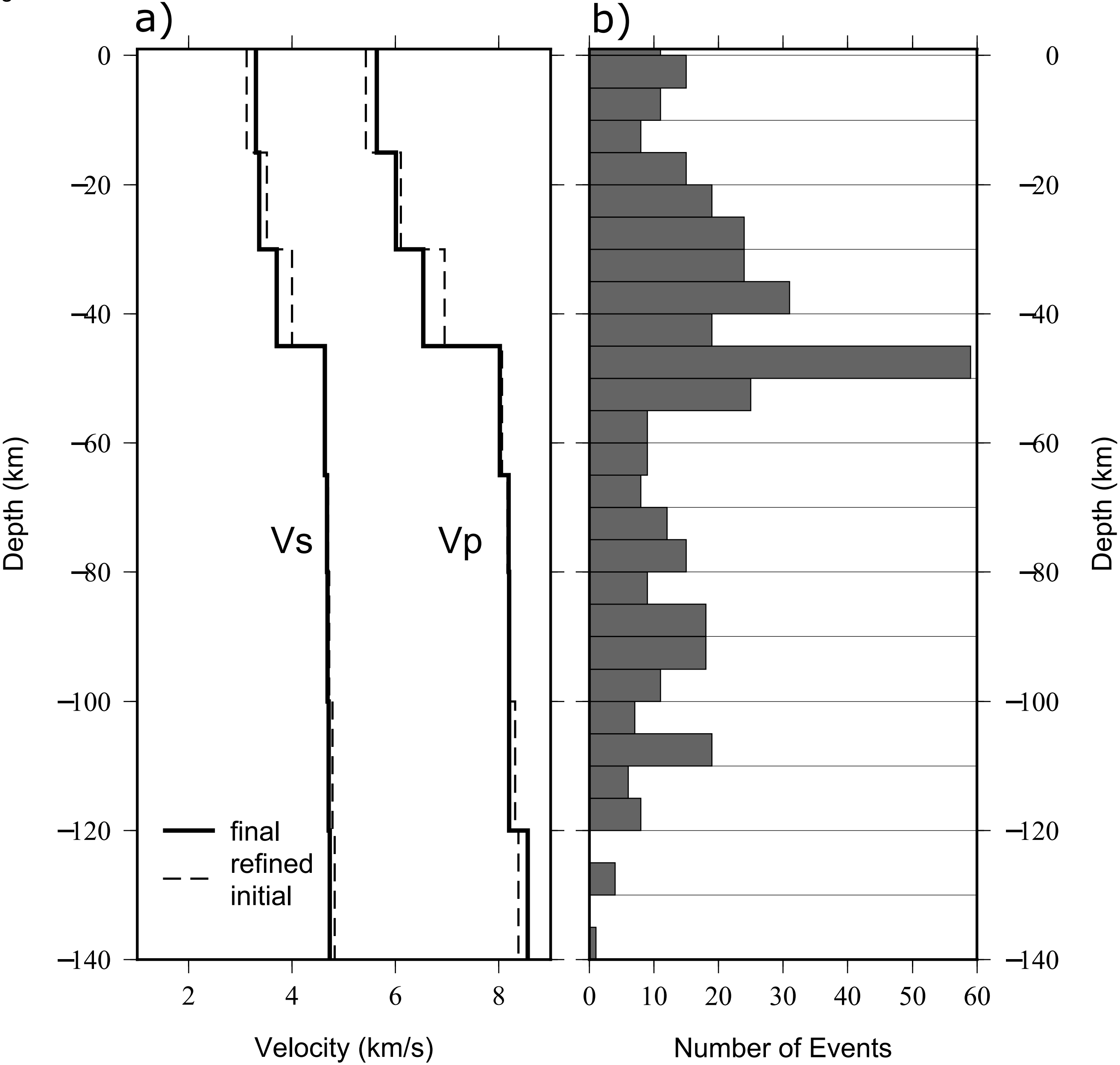

a)
b)
0
–20
–40
–60
–80
–100
–120
–140
Depth (km)
Vs
Vp
final
refined
initial
2
4
6
8
Velocity (km/s)
0
10
20
30
40
50
60
Number of Events

Figure6

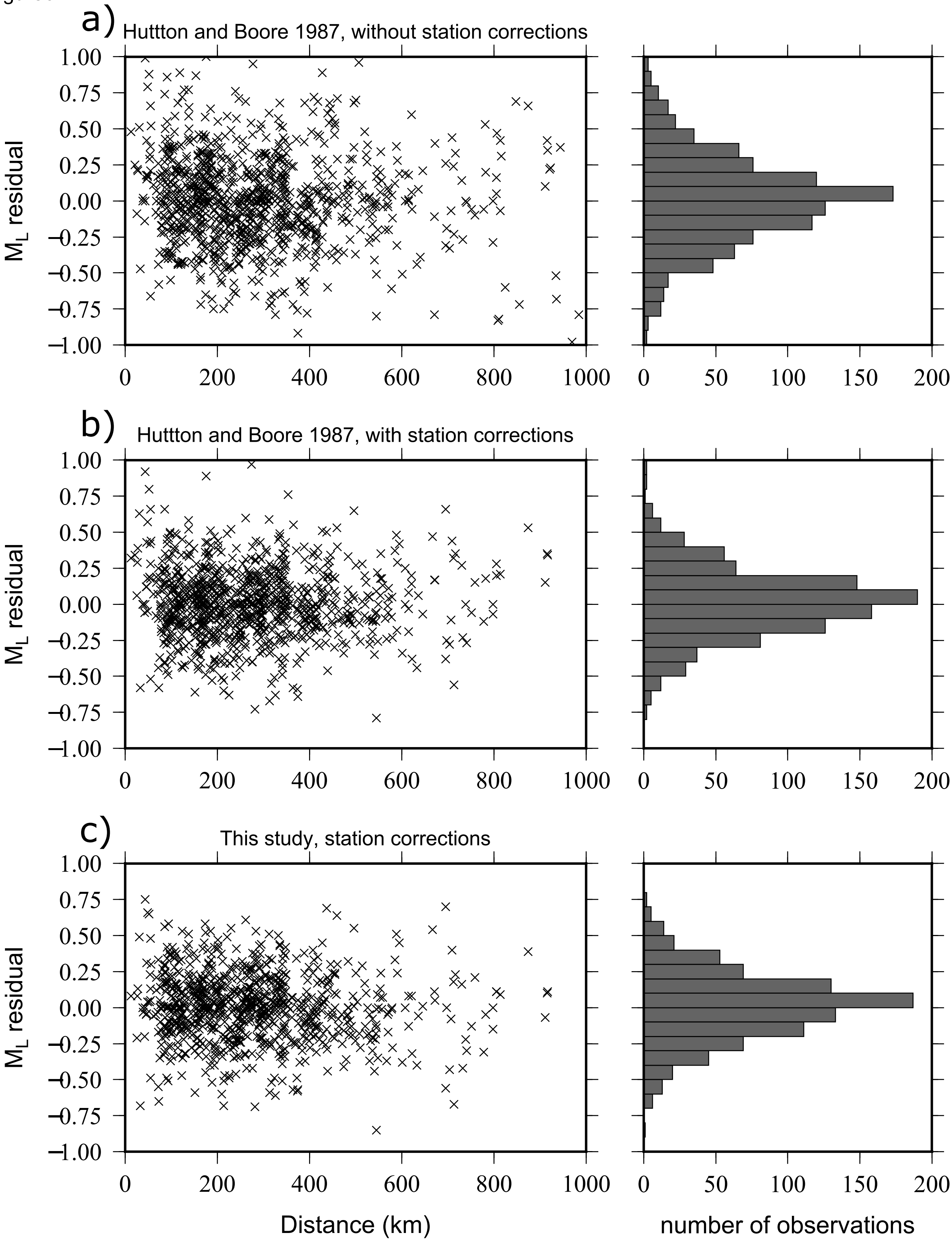
a)
Huttton and Boore 1987, without station corrections
b)
Huttton and Boore 1987, with station corrections
c)
This study, station corrections
M_L residual
1.00
0.75
0.50
0.25
0.00
−0.25
−0.50
−0.75
−1.00
0
200
400
600
800
1000
50
100
150
Distance (km)
number of observations

Figure7

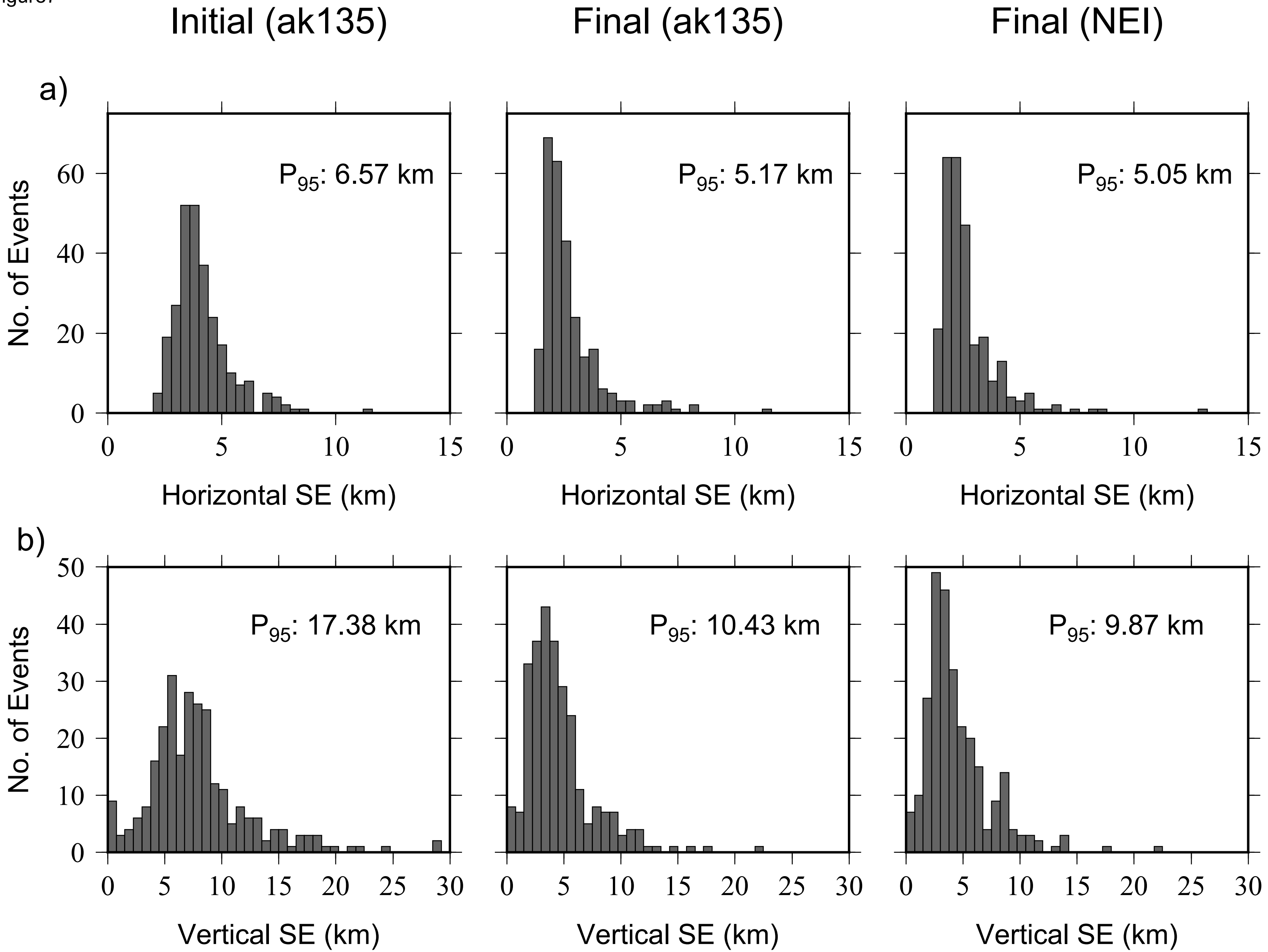
Initial (ak135)
Final (ak135)
Final (NEI)
a)
P95: 6.57 km
P95: 5.17 km
P95: 5.05 km
No. of Events
Horizontal SE (km)
Horizontal SE (km)
Horizontal SE (km)
b)
P95: 17.38 km
P95: 10.43 km
P95: 9.87 km
No. of Events
Vertical SE (km)
Vertical SE (km)
Vertical SE (km)

Figure8

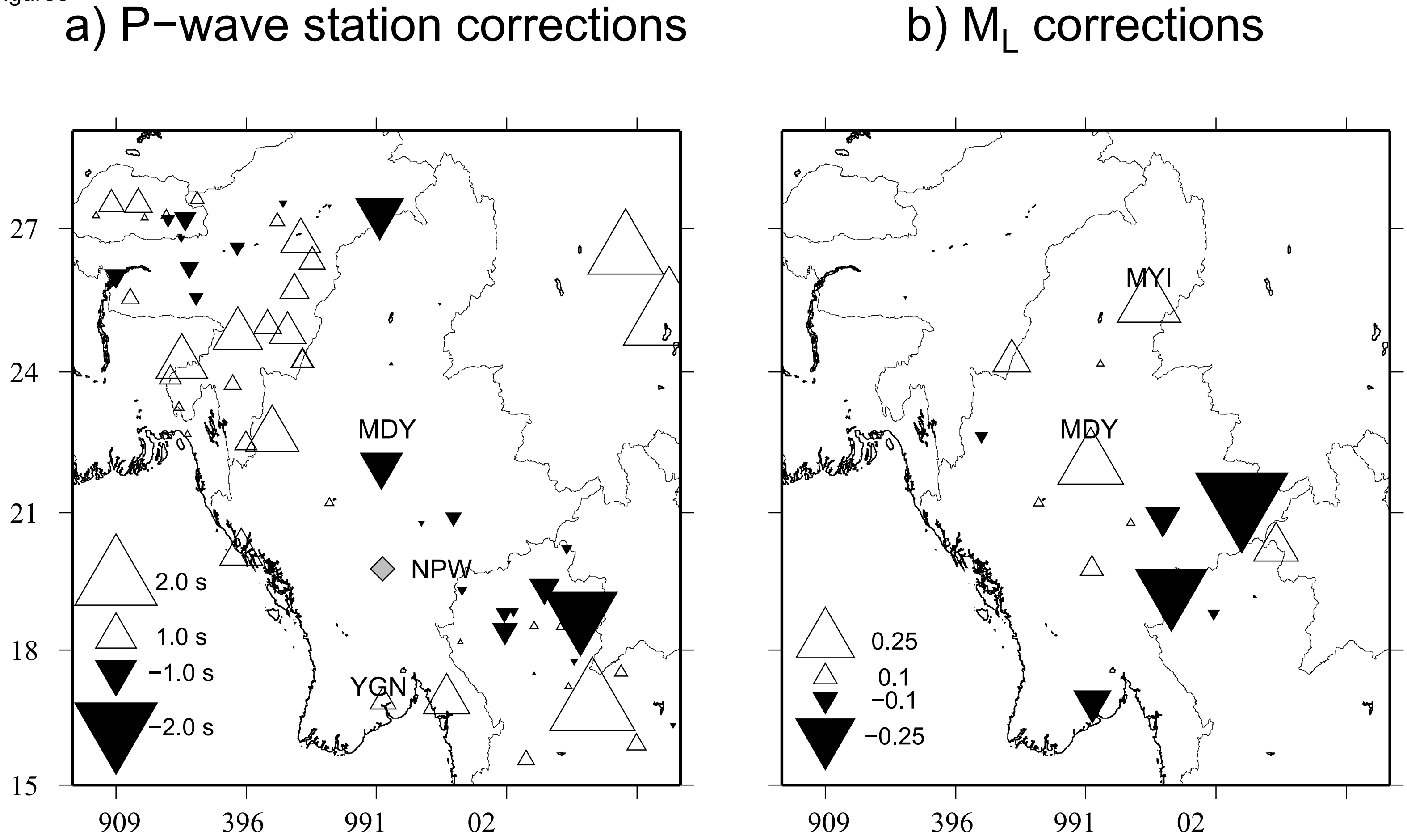
a) P−wave station corrections
b) M_L corrections
MDY
NPW
YGN
MYI
MDY
2.0 s
1.0 s
−1.0 s
−2.0 s
0.25
0.1
−0.1
−0.25
27
24
21
18
15
909
396
991
02
909
396
991
02

Figure9

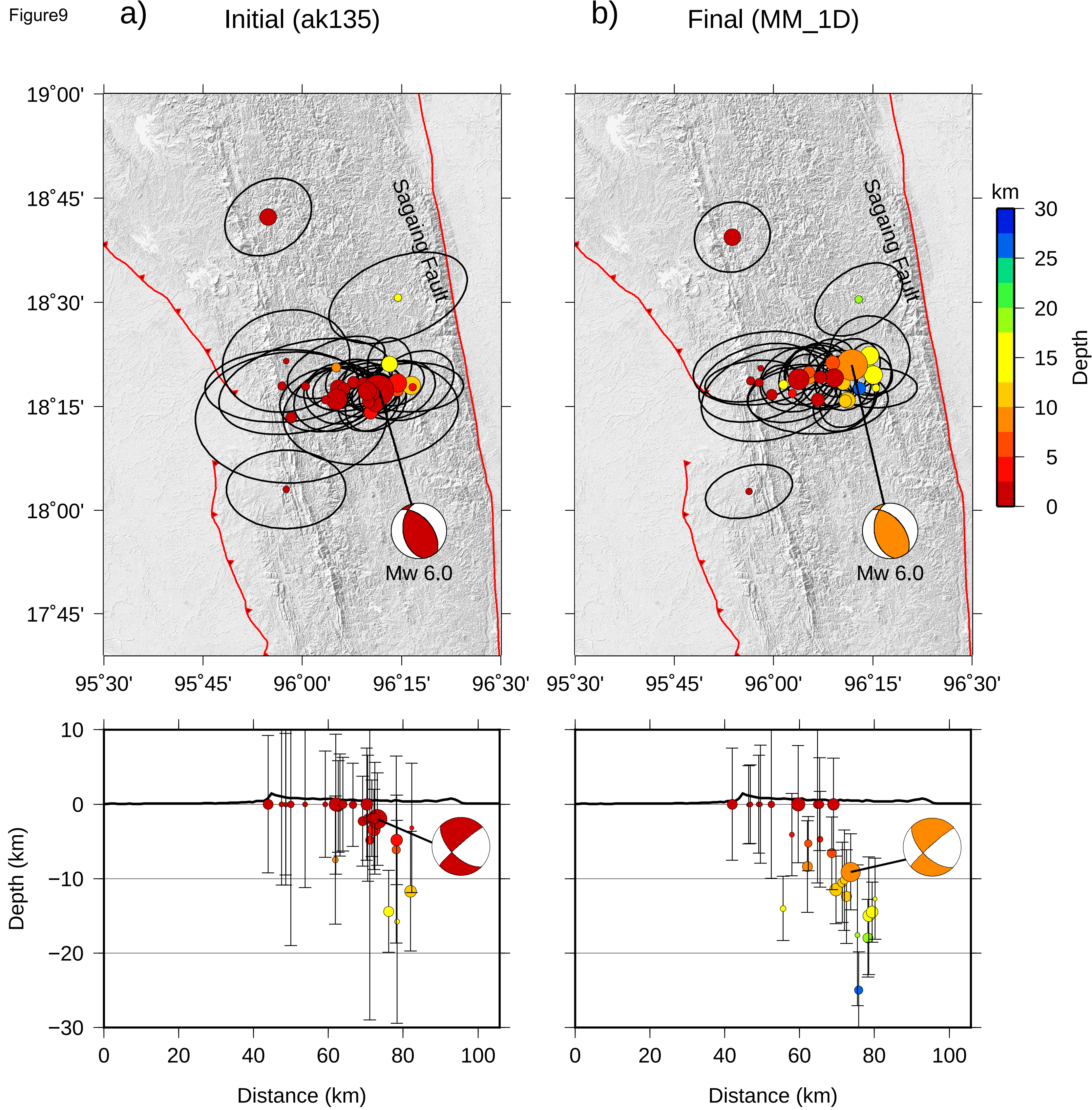

a)
Initial (ak135)
b)
Final (MM_1D)
19°00'
18°45'
18°30'
18°15'
18°00'
17°45'
95°30'
95°45'
96°00'
96°15'
96°30'
Sagaing Fault
Mw 6.0
km
30
25
20
15
10
5
0
Depth
Depth (km)
10
0
−10
−20
−30
0
20
40
60
80
100
Distance (km)

Figure10

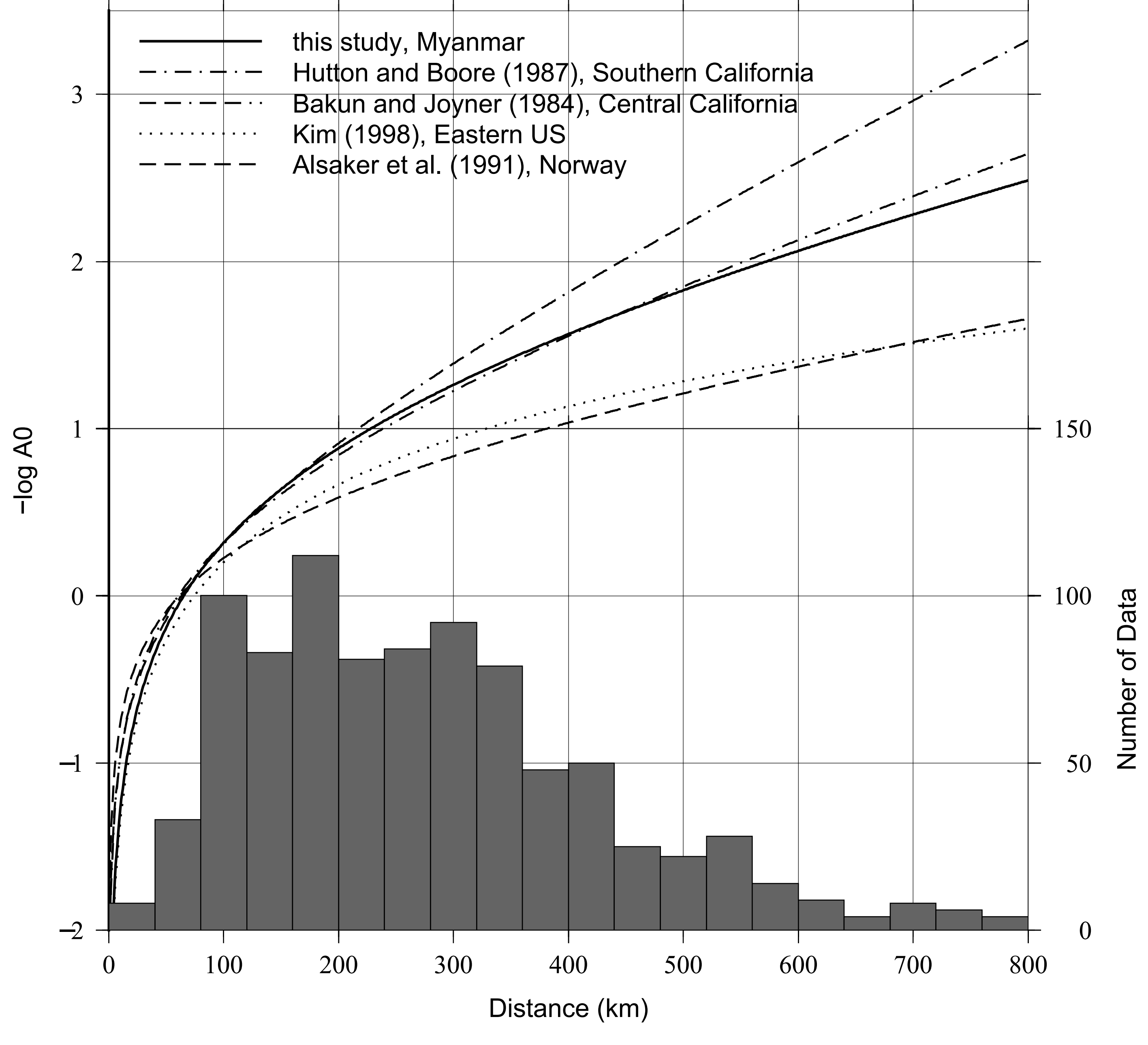

this study, Myanmar
Hutton and Boore (1987), Southern California
Bakun and Joyner (1984), Central California
Kim (1998), Eastern US
Alsaker et al. (1991), Norway
3
2
1
0
−1
−2
−log A0
150
100
50
0
Number of Data
0
100
200
300
400
500
600
700
800
Distance (km)

Electronics Supplement to

Minimum 1D Velocity Model and Local Magnitude Scale for Myanmar

Hasbi Ash Shiddiqi[1], Pa Pa Tun[2], Lars Ottemöller[1]

[1]Department of Earth Science, University of Bergen, Allègaten 41, N-5007 Bergen, Norway.

[2]Department of Meteorology and Hydrology, Office No. 5, Ministry of Transport and Communications, Zeya Htani Road, Nay Pyi Taw, Myanmar.

This electronic supplement contains the figures that show initial velocity models used for the 1D velocity inversion, travel-delays for P- and S-waves, comparison of 602 earthquakes located using the final velocity model, and the comparison of local magnitude residual of shallow and deep events. Tables for the travel-time delays and local magnitude station corrections are also included in this supplementary in CSV format.

Figures:

Figure S1. Initial seismic velocity models used in the inversion

Figure S2. P-wave (a) and S-wave (b) station corrections.

Figure S3. a. Epicenter distribution of the 602 earthquakes in Myanmar located using the final velocity model. Black boxes are the locations of the cross-sections. Cross-section of 602 earthquakes in Myanmar located using the ak135 (b) and the MM_1D (b) velocity models. The subduction slab geometries from slab2 model (Hayes *et al.*, 2018) are shown as black dashed lines.

Figure S4. a. Comparison between M_L Myanmar and M_L Southern California (SoCal), both magnitudes use stations corrections. b. Differences between M_L Myanmar and M_L Southern California.

Figure S5. The orthogonal linear regression results between M_L Myanmar and mb (ISC) for 73 earthquakes. The center solid line is the regression, and the dashed lines are the lines of orthogonal standard error (±0.23 magnitude unit).

Figure S6. a. M_L residuals with respect to distance for shallow (depth $\leq$ 50 km) and deep (depth > 50 km) events. b. M_L residuals vs number of observations for shallow and deep events.

Tables (in CSV format):

Table T1. P- and S-waves station corrections.

Table T2. Local magnitude station corrections.

Reference

Hayes, G. P., G. L. Moore, D. E. Portner, M. Hearne, H. Flamme, M. Furtney, and G. M. Smoczyk (2018). Slab2, a comprehensive subduction zone geometry model, *Science.* **362**, no. 6410, 58–61, doi: 10.1126/science.aat4723.

Supplemental Material (FigureS1)

Click here to access/download;Supplemental Material (Main Page, Tables, and Figures);figureS1.pdf

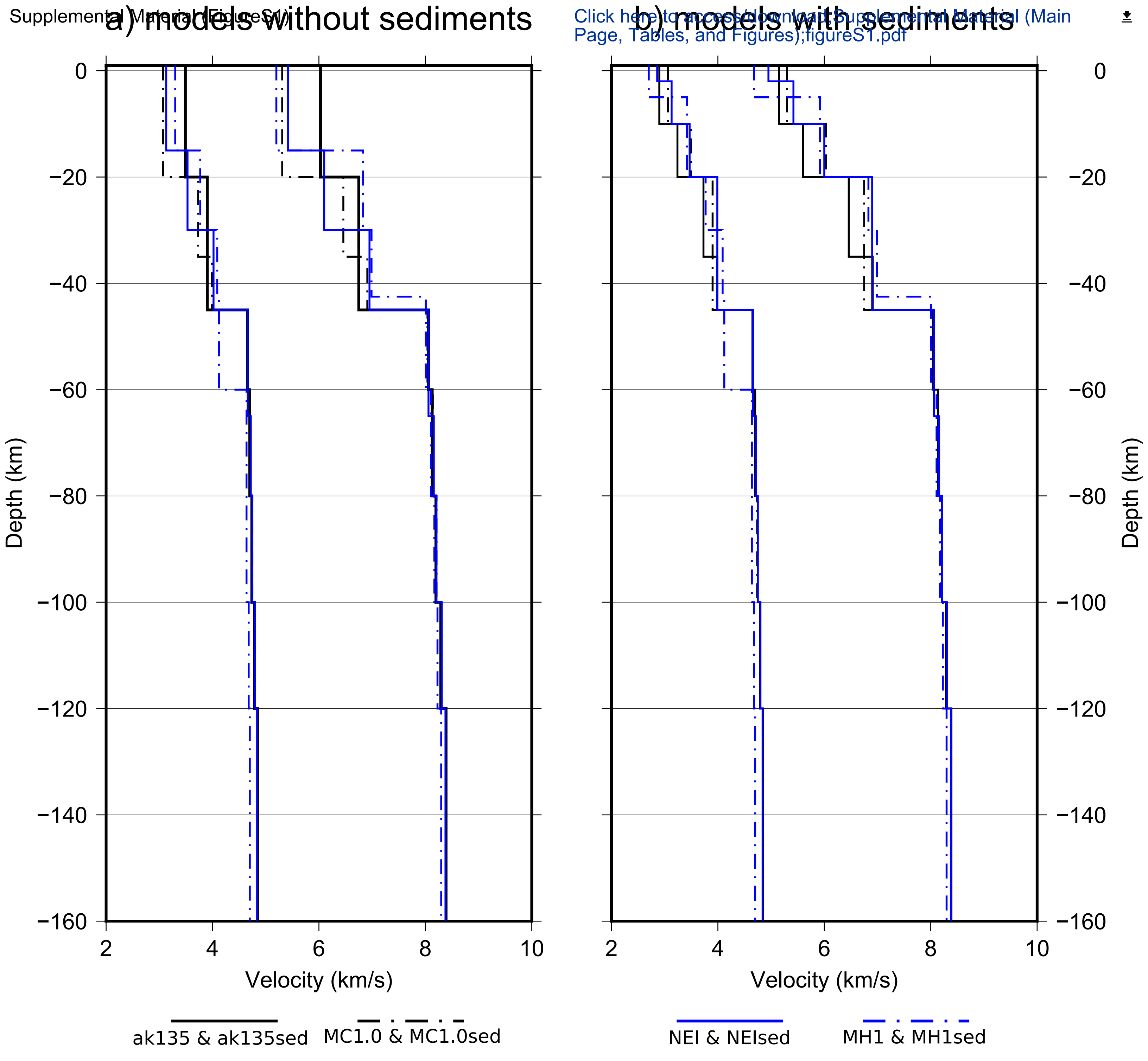

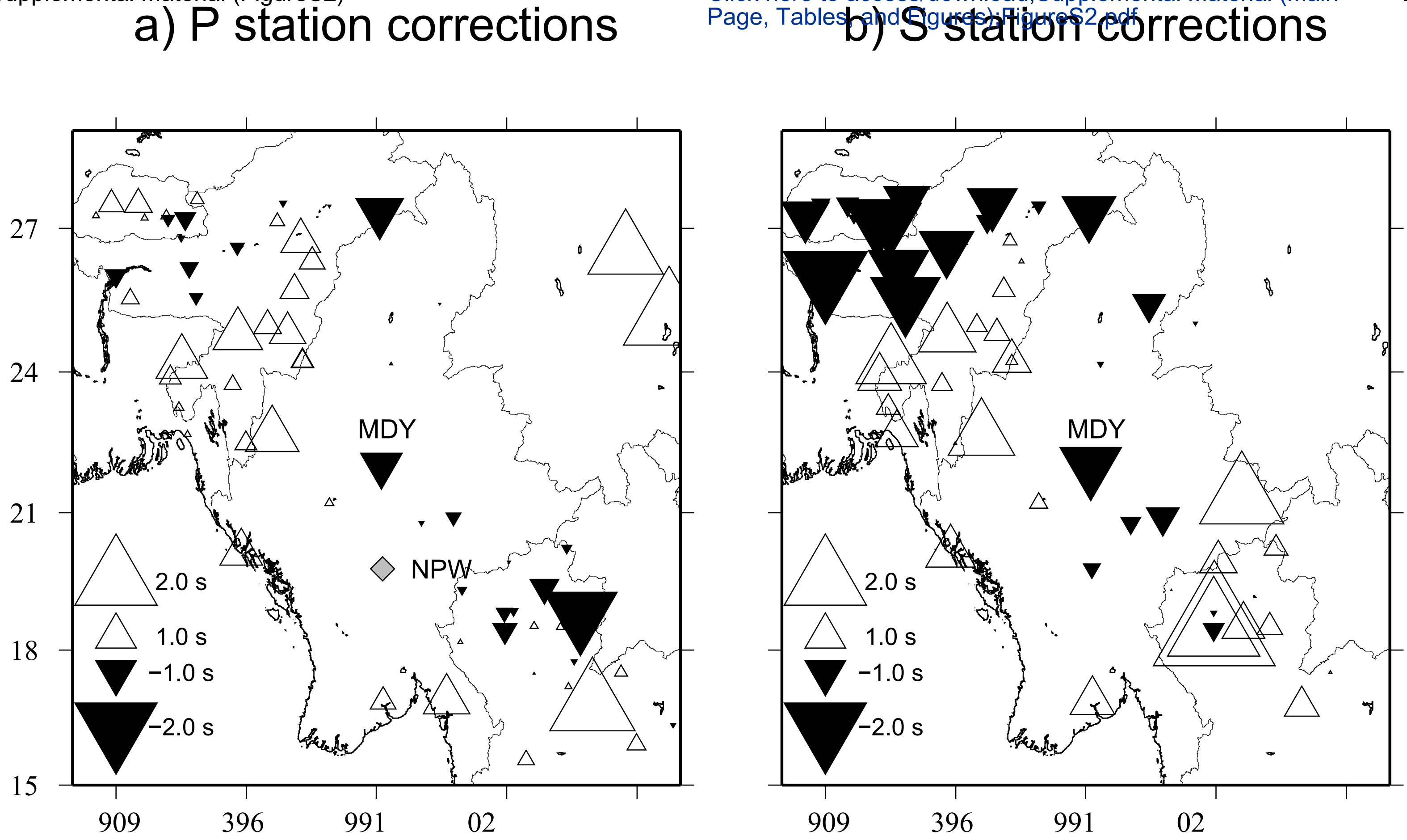
a) P station corrections
b) S station corrections
MDY
NPW
2.0 s
1.0 s
−1.0 s
−2.0 s
27
24
21
18
15
909
396
991
02

Supplemental Material (FigureS3)

Click here to access/download;Supplemental Material (Main Page, Tables, and Figures);FigureS3.pdf

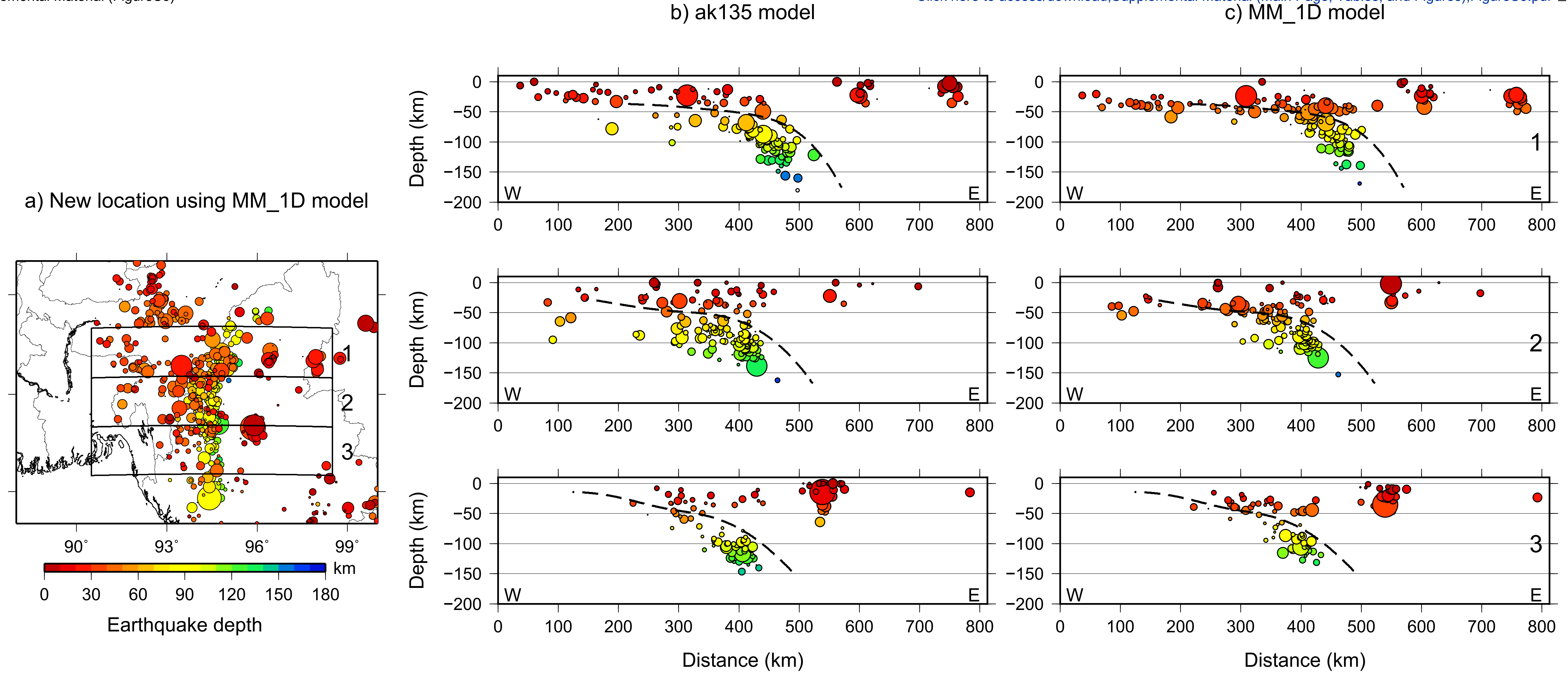

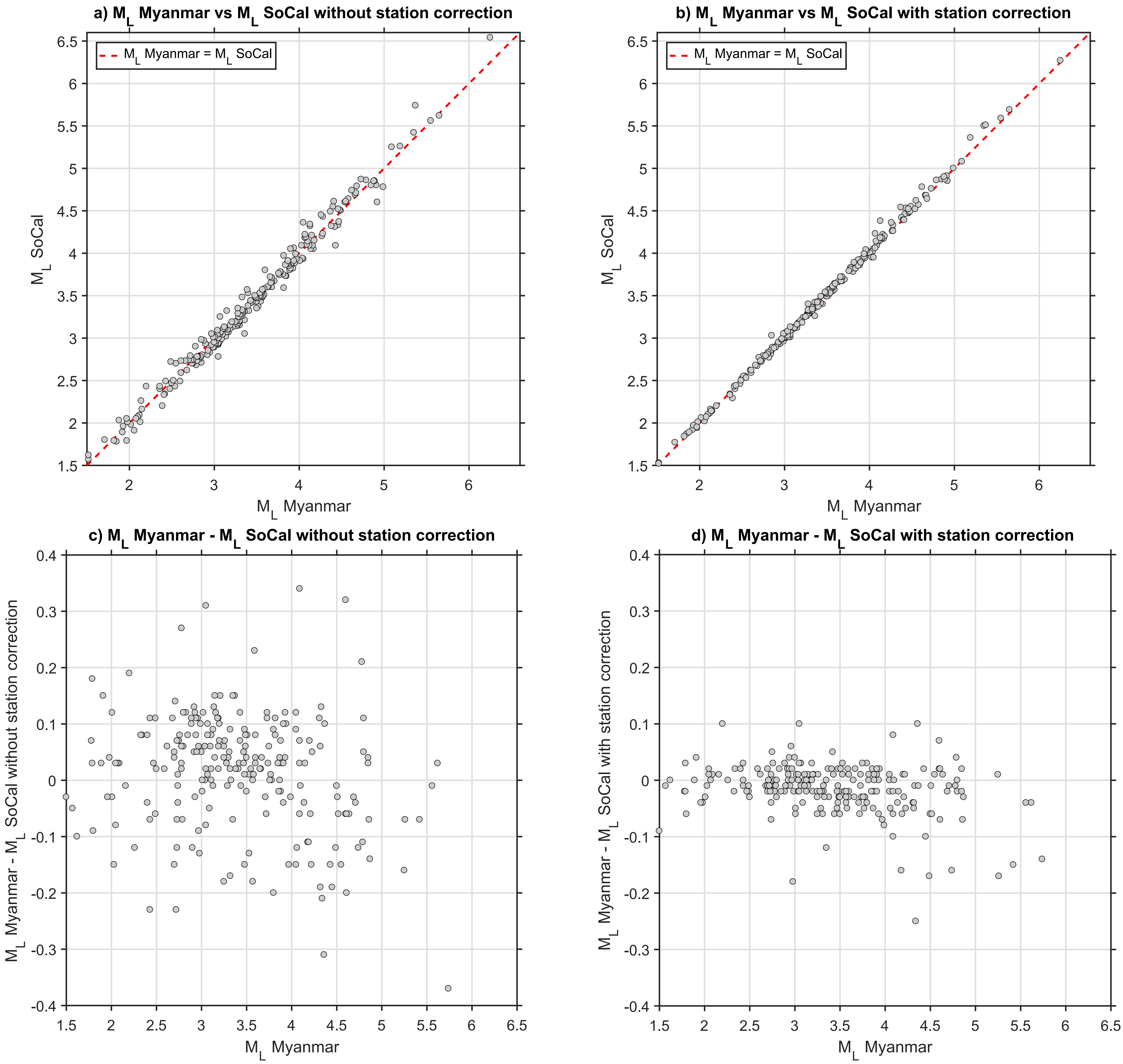

a) M_L Myanmar vs M_L SoCal without station correction
b) M_L Myanmar vs M_L SoCal with station correction
M_L Myanmar = M_L SoCal
M_L SoCal
M_L Myanmar
c) M_L Myanmar - M_L SoCal without station correction
d) M_L Myanmar - M_L SoCal with station correction
M_L Myanmar - M_L SoCal without station correction
M_L Myanmar - M_L SoCal with station correction

Supplemental Material (FigureS5)

Click here to access/download;Supplemental Material

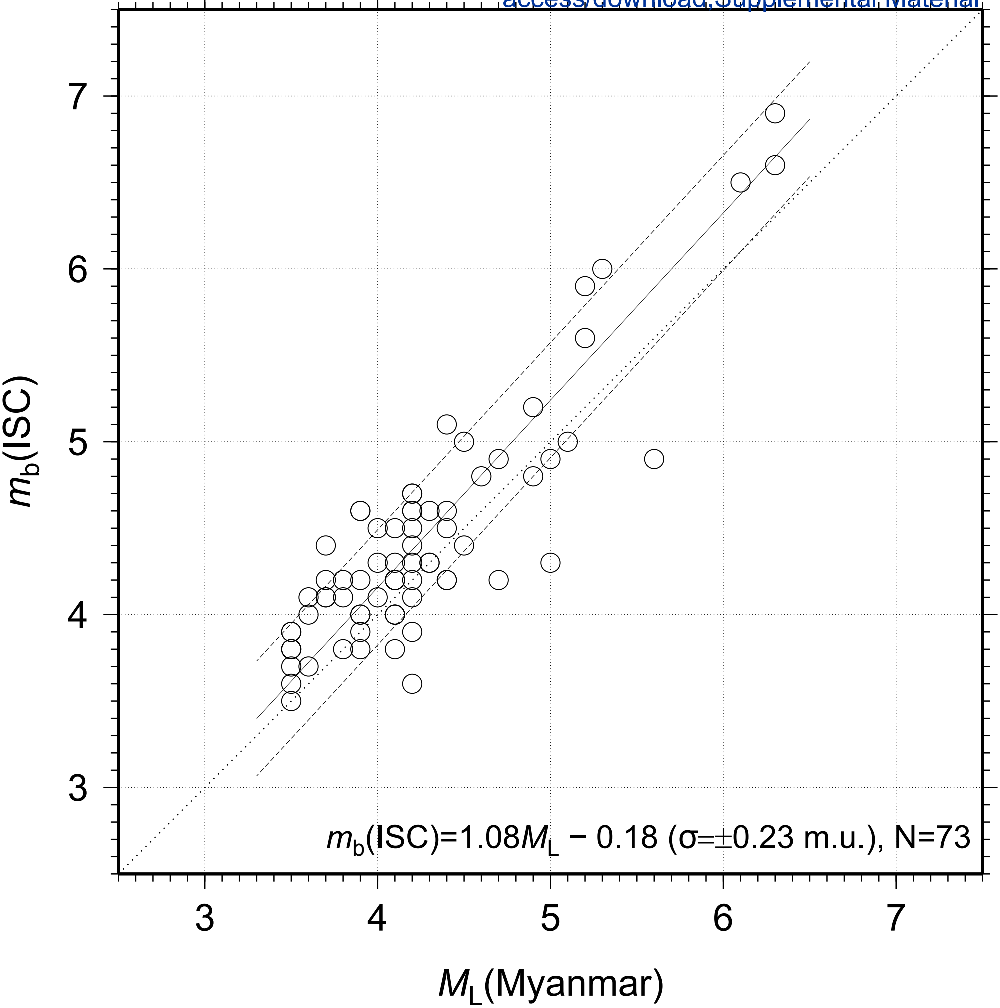

Supplemental Material (FigureS6)

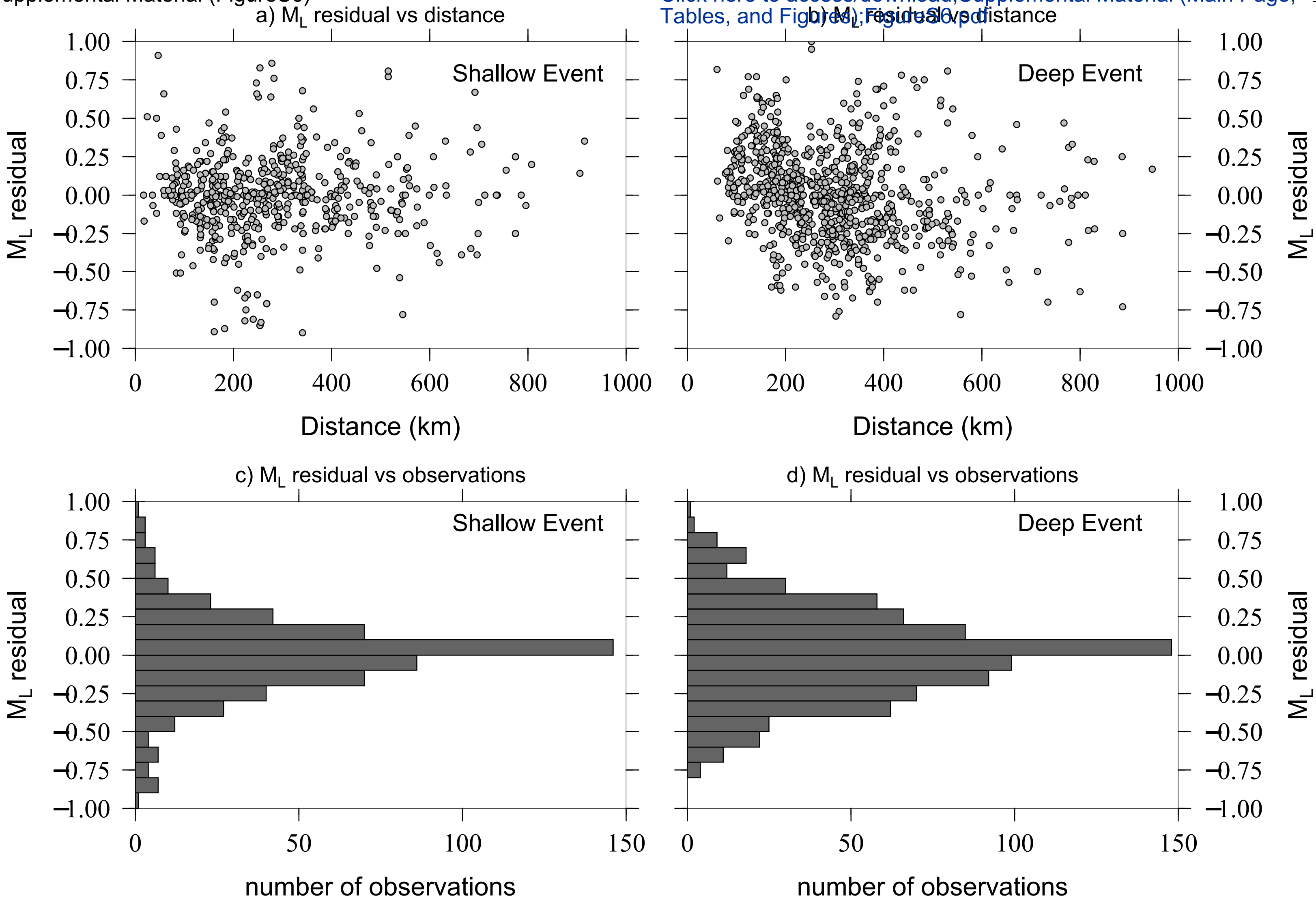

Click here to access/download

Supplemental Material (All Other Files, i.e. Movie, Zip, csv)

TableT1.csv